

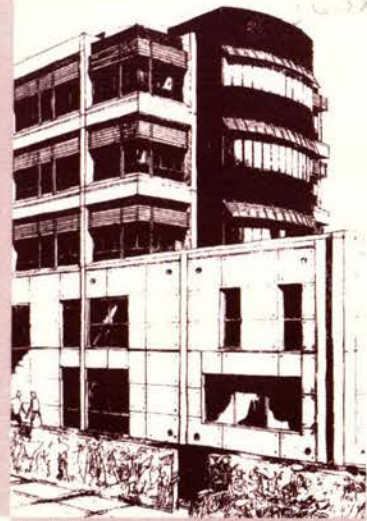
S&G 3608

# Research Report

2000 - 2

March 2000

ISSN 0110 - 3326



A Report to EQC on

## A Two-Dimensional Study of the Seismic Response of the Aburrá Valley, Medellín, Columbia

Brian Adams  
Rob Davis  
John Berrill

**Civil Engineering**



A Report to EQC on

**A TWO-DIMENSIONAL STUDY ON THE  
SEISMIC RESPONSE OF THE ABURRÁ VALLEY,  
MEDELLÍN, COLOMBIA**

Brian Adams  
Rob Davis  
John Berrill  
Department of Civil Engineering  
University of Canterbury

March 2000

---

## PREFACE

---

This report presents the results of an investigation into the propagation of seismic waves within the Aburrá Valley, Medellín, Colombia. The research was made possible with information collected during a short trip to Colombia by the first author, Brian Adams, a Ph.D. student in Civil Engineering at the University of Canterbury. Mr Adams was based at the Universidad EAFIT in Medellín, Colombia between 14 and 30 August 1999. During this time he also made a brief visit to Armenia, Colombia to inspect damage from a recent strong earthquake in January 1999. The research was initially proposed both by the authors and Professor Juan Diego Jaramillo of the Universidad EAFIT, a visiting academic at the University of Canterbury in 1999. Travel expenses were kindly funded by the Earthquake Commission of New Zealand (EQC) and the New Zealand Society for Earthquake Engineering (NZSEE). Subsequent numerical modelling was carried out between September 1999 and February 2000 at the University of Canterbury.

---

## ABSTRACT

---

A two-dimensional elastic finite-element method is used to investigate the seismic response of the Aburrá Valley of Medellín, Colombia. A vertically propagating anti-plane SH Ricker wavelet is used to study the response of the valley for frequencies up to 5Hz. The Aburrá Valley is very large and geologically diverse. The ~1200-metre-deep and ~15-kilometre-wide valley is covered by a variable layer of soft soils averaging some 30 metres deep. The soils are mainly residual, alluvial or debris-flow deposits. The valley also contains a network of 24 strong-motion seismic recorders. A 49,900-element mesh of a cross-sectional model through the southern end of Medellín is analysed using the finite-element software package, Archimedes. The results are presented in both time and frequency domains. A similar one-dimensional finite-element method is used for comparison. It is found that while amplification often occurs at frequencies defined by a one-dimensional analysis, the level of amplification is often highly dependent on multi-dimensional effects. Local irregularities in the stratigraphy and topography at some sites have a significant effect on the seismic response. Site response may also be influenced strongly by sub-valley structures up to a few kilometres across, yet the influence of the valley as a whole is small. Poor correlation between modelling results and recorded data is probably due to a lack of site-specific detail within the model, and the limiting two-dimensional nature of the analysis.



---

# CONTENTS

---

<b>Chapter 1: INTRODUCTION.....</b>	<b>7</b>
1.1 PHYSICAL SETTING .....	7
1.2 COLOMBIAN TECTONICS .....	8
1.3 THE ABURRÁ VALLEY AND MEDELLÍN.....	9
<b>Chapter 2: THE MEDELLÍN INSTRUMENTATION AND MICROZONATION PROJECT .....</b>	<b>13</b>
2.1 SEISMIC RISK TO THE CITY OF MEDELLÍN.....	13
2.2 ACCELEROGRAPH NETWORK DATA .....	16
2.3 ABURRÁ VALLEY GEOLOGY .....	18
2.4 GEOLOGICAL AND GEOTECHNICAL DATA.....	24
<b>Chapter 3: METHOD OF ANALYSIS.....</b>	<b>25</b>
3.1 ABURRÁ VALLEY CROSS-SECTION AND TWO-DIMENSIONAL MODEL .....	25
3.1.1 <i>Geological Units within the Model</i> .....	28
3.1.2 <i>Near-Surface Stratigraphy</i> .....	28
3.1.3 <i>Model Geometry at the Accelerograph Stations</i> .....	31
3.2 TWO-DIMENSIONAL FINITE ELEMENT METHOD .....	34
3.2.1 <i>The Finite Element Algorithm</i> .....	36
3.2.2 <i>Material Damping</i> .....	37
3.2.3 <i>Input Signal</i> .....	37
3.2.4 <i>Absorbing Boundary</i> .....	39
3.3 ONE-DIMENSIONAL FINITE ELEMENT METHOD .....	39
3.4 POST-PROCESSING .....	40
<b>Chapter 4: RESULTS .....</b>	<b>43</b>
4.1 TIME-DOMAIN ANALYSIS.....	43
4.1.1 <i>Amplification of the First Arrival</i> .....	43
4.1.2 <i>Surface wave action</i> .....	47
4.1.3 <i>Vertical Wave Reflection and Resonance within the Soft Layers</i> .....	47
4.1.4 <i>Errors due to Incomplete Absorption at the Artificial Boundary</i> .....	48
4.1.5 <i>Transient Response in the Region of the Accelerograph Stations</i> .....	49
4.2 SPECTRAL ANALYSIS .....	53
4.2.1 <i>A Comparison Between One- and Two-Dimensional Analyses</i> .....	53
4.2.2 <i>Frequency Response in the Region of the Accelerograph Stations</i> .....	56
4.3 COMPARISON WITH RECORDED DATA .....	58
4.3.1 <i>Recorded Weak Motions</i> .....	58
4.3.2 <i>Accelerograph Station UEA</i> .....	59
4.3.3 <i>Accelerograph Station ISA</i> .....	62
4.3.4 <i>Accelerograph Station EET</i> .....	62

**Chapter 5: DISCUSSION .....63**

**Chapter 6: CONCLUSIONS .....69**

**ACKNOWLEDGMENTS .....71**

**REFERENCES.....73**

---

## Chapter 1: INTRODUCTION

---

The seismic site response of non-uniform near-surface geology such as sediment-filled basins and topographic ridges and valleys is of great interest to a geologically diverse and tectonically active country like New Zealand. Such complex geology often leads to serious multi-dimensional amplification effects such as focussing, basin resonance, and edge effects. These amplifications cannot be modelled nor predicted with simple one-dimensional analyses as is commonly used in engineering design.

The South American country of Colombia also fits the geologically diverse and tectonically active description very well, and contains many sites of interest. One of these is the City of Medellín in the Aburrá Valley, which in addition to complex near-surface geology, contains the largest local network of accelerographs in South America. Anomalously high levels of ground motion at several of these accelerograph stations indicate that the seismic response is probably dominated by multi-dimensional amplifications.

In this study we use two-dimensional elastic finite-element modelling techniques to investigate the seismic response across the width of the Aburrá Valley. A similar method was used by the authors in a study two-dimensional seismic response study of the much smaller Wellington-Hutt Valley basin in New Zealand (Adams et. al, 1999). In the Lower Hutt it was found that both the deep sedimentary structure and the sharp basin edge had a significant effect on the seismic response of the whole valley. The general aims of this study are to firstly determine if two-dimensional effects are likely to dominate the seismic response of the valley as a whole; to secondly look for areas where multi-dimensional focussing or edge effects might generate locally high amplifications; and to thirdly compare our elastic analysis results with those obtained from recorded weak motions at some of the accelerograph sites.

### *1.1 PHYSICAL SETTING*

Colombia is the north-western-most and fourth-largest country in South America, bordering with Panama and the Caribbean Sea to the north, Venezuela and Brazil to the east, Peru and Ecuador to the south, and the Pacific Ocean to the west. Colombia has a land area of

1,141,748 km<sup>2</sup> and a population of 37.5 million. The western half of the country is mountainous, containing three parallel branching cordillera (mountain ranges) of the Northern Andes, while the eastern territory is extensive lowland jungle of the great Orinoco and Amazon basins. With its diverse and rugged geography, Colombia is a land frequented by natural disasters, with many historical episodes of flooding, hurricanes, earthquakes, volcanic eruptions, tsunami and avalanches.

Medellín is Colombia's second largest city and the capital of the Department of Antioquia. It has a population of 1.8 million (June 1995), and an urban area of 110 km<sup>2</sup> spectacularly located in the deep Aburrá Valley, a 1200 metre deep depression in the surrounding highlands. The Aburrá Valley is located in north-west Colombia, in the Central Cordillera of the Northern Andes. The central business district (CBD) of Medellín (figure 1.1) is located in the bottom of the Aburrá Valley at an altitude of 1500 metres, while the surrounding rolling countryside of the cordillera lies at an altitude between 2600 and 2800 metres. The urban area extends to a length of 25km and a width of 5-10km.



*Figure 1.1. Photograph of the central business district (CBD) of Medellín in the bottom of the deep Aburrá valley. As viewed from Cerro Nutibara (see figure 1.3).*

## **1.2 COLOMBIAN TECTONICS**

Colombia is located in the north-west corner of the South American continent, near the boundary of the Nazca, Caribbean and South American tectonic plates, as well as the smaller

Costa Rica-Panama microplate and the North Andes block (figure 1.2). In general, the Nazca plate is moving to the east at some  $\sim 50\text{mm/year}$  and is subducting beneath the South American plate at the Colombian Trench. The Caribbean Plate is moving southward at  $\sim 8\text{mm/year}$  and is slowly subducting beneath Colombia from the north (Mora, 1995). This has resulted in a tectonic regime of compression, uplift and sinistral strike-slip movement within the North Andes block of western Colombia. The North Andes block itself is moving at a rate of some  $\sim 6\text{mm/year}$  north-east relative to the stable South American plate with dextral slip along north-east trending Eastern Andean Frontal Fault Zone which originates in the Gulf of Guayaquil (Monsalve and Mora, 1999).

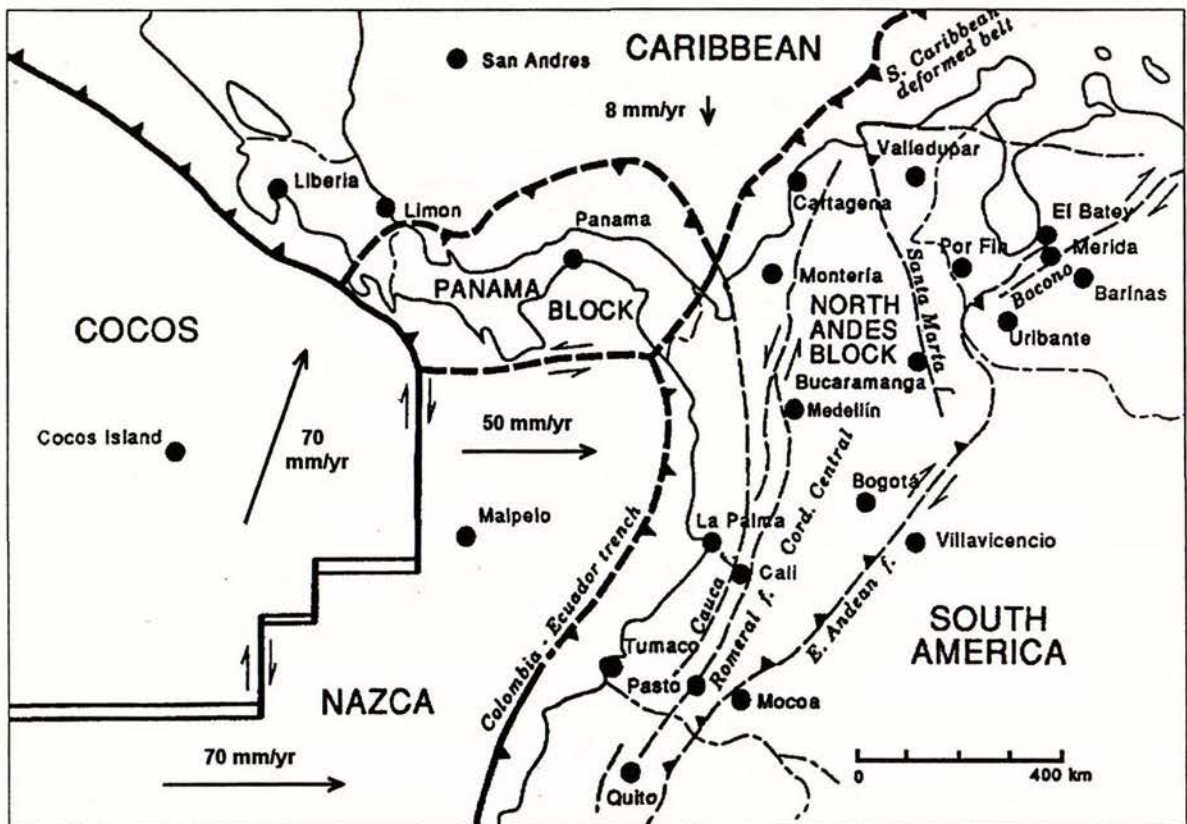
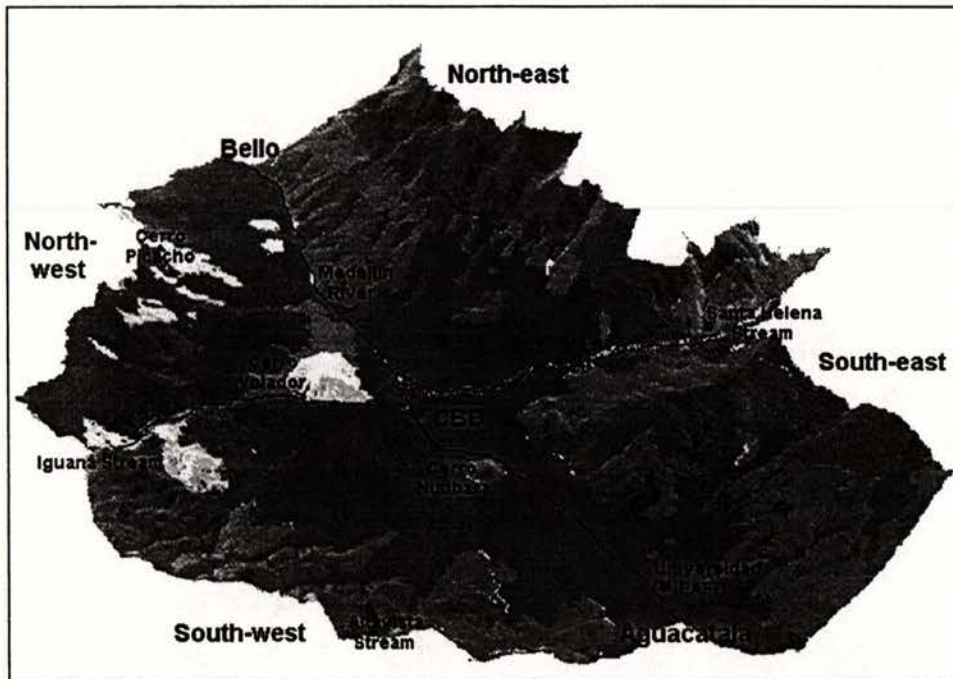


Figure 1.2. Tectonic plate interactions in north-west South America showing directions and rates of plate movements relative to the South American plate (after Kellogg and Dixon, 1990).

### 1.3 THE ABURRÁ VALLEY AND MEDELLÍN

The Aburrá Valley drains north to north-east for 200km into the Cauca River and then to the Caribbean Sea some 500km away. The city of Medellín (figures 1.3 and 1.4) is located only 20km from the head of the valley, with the Medellín River flowing north and descending 75

metres over a distance of 13.7km from Aguacatala at 1505m (above mean sea level) down to Bello at 1430m. Both the geomorphology and lithology of the valley are incredibly diverse and variable on both a very local and city-wide scale.



*Figure 1.3. A three-dimensional model of the Aburrá valley (GSM, 1999) at Medellín. The valley is naturally divided into four sectors (NW, NE, SE SW) by the Medellín River and two major side streams.*



*Figure 1.4. A photograph of central Medellín, looking south-west from high above the true right of the Santa Helena Stream*

Two major side valleys enter the Aburrá near the centre of town; the Santa Helena valley from the east and the Iguaná valley from the west. Their effect is to geographically split the city into four sectors (north-west, north-east, south-east, south-west). Numerous other tributaries flow down into the Medellín River, of which the Altavista, Aguas frias o Picacha, Ana Díaz and La Hueso creeks on the south-western flank have the most influence on topography. There is very little completely flat land within the city, with the sides gently sloping up from the river, and steepening toward the crest of the bordering hills.

A large percentage of the valley is covered by residential, industrial and commercial buildings (figures 1.5 and 1.6). The CBD (figure 1.1) is located on alluvial deposits from the Medellín River and the Santa Helena Stream. Here there is a cluster of buildings in the 20-40 storey range. The local airport lies on alluvial material on the south-west side of the valley. Much of the population lives in multi-storey apartment buildings up to 20 stories in height, but generally in the 4-8 storey range. Many also live in single or double-storey single-family dwellings. Higher up the slopes, and in the northern end of the valley, the construction appears to be of a much poorer standard, and often of unreinforced hollow-core masonry.

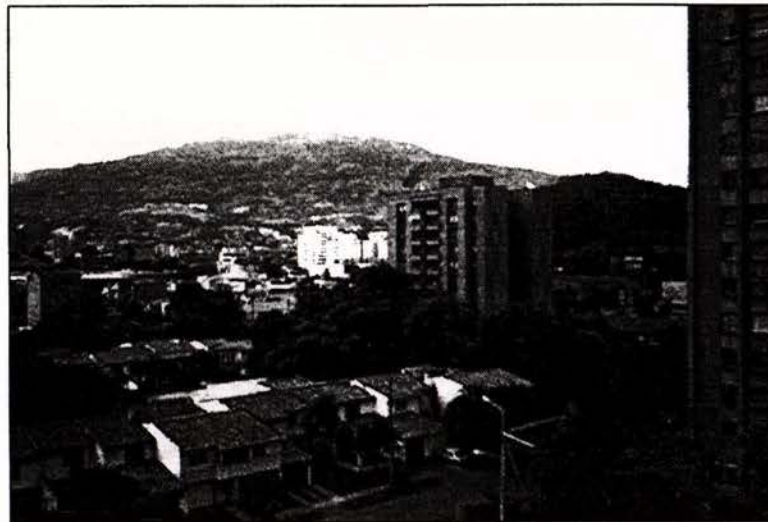


*Figure 1.5. The 16-storey apartment buildings of Suramericana on alluvial deposits of the lower Iguaná Stream. Double-storey residential housing in the foreground. In the background the vegetated Cerro Volador lies to the front right of the north-west flank.*

Moment resisting reinforced concrete frames are the most common form of construction for large buildings. Both reinforced and unreinforced masonry is commonly found in both apartment buildings and single-storey houses (García, 2000). Colombia's first mandatory earthquake resistant legislation was passed into law in 1984 (García, 1984). This introduced

the use of structural walls, and forbade further construction with unreinforced masonry. There are, however, still a large number of unreinforced masonry buildings in existence. Of the engineered masonry buildings, both simple reinforced hollow-core bricks, and confined reinforced masonry (surrounded by a light reinforced concrete frame) are very common (García, 2000). An update to the code in 1998 included requirements for non-structural elements such as the unreinforced brick in-fills that are very common Colombian construction.



*Figure 1.6. An aerial view over urban construction on the lower south-west flank. The residential apartments and low-rise housing shown here have been built on flood, colluvial, alluvial and debris-flow deposits.*

---

## Chapter 2: THE MEDELLÍN INSTRUMENTATION AND MICROZONATION PROJECT

---

Recent damaging earthquake in Medellín, in November 1979 and October 1992, sparked the start of a comprehensive study of earthquake risk in the city. In 1993, a preliminary seismic risk study by the Universidad EAFIT (Velásquez, E. and Jaramillo, J.D., 1993; Hincapié, J.E.; Osorio, R.; Pineda, C.M. and Urrea D.P., 1993; Jaramillo, J.D. and Ortega, D.C., 1993) found that a re-occurrence of the 1979 event would cost the city an estimated \$US300 million. It was noted that the damage distribution from the most recent earthquakes had been very erratic and concentrated in certain zones, indicating a very non-uniform shaking pattern. The observations called to the need for a detailed study of the area to aid in the safe and efficient seismic design of the city and its infrastructure.

An interdisciplinary group was formed called the *Grupo de Sismología de Medellín* (GSM). This included the Universidad EAFIT, the Faculty of Mining at the Universidad Nacional de Colombia, INGEOMINAS (National Institute of Geo-Sciences, Mining and Chemistry) and INTEGRAL S.A. (A South American consulting engineering firm based in Medellín). The Grupo de Sismología de Medellín was given the Instrumentation and Microzonation Project by SIMPAD (System for the Prevention and Attention of Disasters in Medellín), appointed by the Private Secretary of the Medellín Municipal.

The results of the Instrumentation and Microzoning Project include:

- A re-evaluation of the seismic risk for the city.
- The installation of a 24 instrument-strong accelerograph network and the subsequent capturing of a large amount of weak motion data.
- Geology and geomorphology maps of the city to a scale of 1:10,000.
- A three-dimensional geotechnical model of the sub-surface geology down to bedrock.
- A seismic microzonation map of the city to a scale of 1:10,000.

### 2.1 SEISMIC RISK TO THE CITY OF MEDELLIN

Seismic activity in Colombia consists both of shallow and deep events along the various subduction interfaces, and shallow crustal events within the tectonic plates. Figure 2.1 shows

the three main sources of seismic activity in Colombia that are close enough to affect the city of Medellín. The first is the Murindó Seismic Zone, approximately 160km north-west of Medellín. Seismicity in this zone is probably a result of collision between the Panama microplate and the North Andes block (Monsalve and Mora, 1999), with some interaction from the subducting Nazca plate. Most of the earthquakes in this zone have a hypocentral depth of less than 35km although some occur deeper than 70km. Both strike-slip and thrust events appear to occur along several prominent fault systems. The second seismic source is the Bucaramanga Nest, located some 280km east of Medellín, below the Cordillera Oriental. This is the origin of the greater part (41%) of Colombia's seismic activity. Most events originate from a depth of 120-160km and have a diverse range of focal mechanisms. The third source of importance is the Viejo Caldas Seismic Zone, some 100-200km south of Medellín. Viejo Caldas activity comes from depths between 35 and 150km and is related to the subduction of the Nazca plate.



Figure 2.1. Showing the three main earthquake sources likely to affect the city of Medellín.

Additional seismic activity in the Viejo Caldas area originates from surficial sources such as the Romeral and Palestina fault systems. The 600km-long north-south trending Romeral fault system (see figure 1.2) of the Central Cordillera extends from Ecuador to northern Antioquia. It has been the source of several of the Colombia's most important earthquakes, including those in Popayán (1983), Páez (1994) and Armenia (1999). Northern branches of the Romeral system lie within 15km of Medellín, yet in recorded history none of these have produced earthquakes with magnitude greater than  $M_S5.0$ .

Historically, Medellín has received only low to moderate strength shaking from both nearby small magnitude earthquakes, and many large-magnitude earthquakes several hundred kilometres distant. Since 1730 there have been reports of 39 earthquakes felt in Medellín with an intensity of MM III or more (GSM, 1999). The most recent of these was the  $M_L6.2$  Armenia earthquake on the 25<sup>th</sup> January 1999 in the coffee growing region of Quindío (Escallón and Alarcón, 2000). This earthquake was centred on the Romeral Fault system 200km south of Medellín, where it was felt with intensity MM III. From these historic earthquakes it is estimated that felt intensity VII shaking in Medellín is equivalent to accelerations of 0.02-0.03g in the rock or ~0.06g at soil sites (GSM, 1999).

The most damaging earthquakes in Medellín in recent history are those of November 1979 and October 1992, during which the maximum acceleration on the rock reached 0.03 and 0.015g respectively. These were large earthquakes yet they both originated some distance away; the 1979 event ( $M_S6.7$ ) from the Viejo Caldas Seismic Zone, and the 1992 event ( $M_S7.2$ ) from the Murindó Fault. Damage occurred in the city during both these events, the latter causing an estimated \$US11 million loss (Fairbaiz et. al., 2000).

The detailed probabilistic analyses have estimated the peak ground accelerations as a function of return period. At a 90% confidence level, a PGA of 0.03g is expected for an earthquake with a return period of 10 years, while a PGA of 0.15g is expected for a 475 year earthquake (GSM, 1997). On top of this, a deterministic analysis was used to evaluate the maximum likely magnitudes and accelerations from a set of worst-case scenario earthquakes. These are shown in table 2.1

Seismic Source	Hypocentral distance (km)	Maximum magnitude ( $M_f$ )	Average acceleration ( $g$ )
Cauca	22	7.0	0.23
Romeral	13	6.9	0.42
La Chillona	9	6.5	0.39
La Sucia	10	6.5	0.39
San Jerónimo	11	6.4	0.36
Espíritu Santo	50	6.2	0.06
Murindó	105	7.6	0.09
Palestina	89	7.0	0.06
Otú Norte	106	7.0	0.05
Viejo Caldas Subduction	115	7.5	0.05
Local Subduction	67	7.0	0.07
Deep Subduction	20	6.5	0.19

Table 2.1 Worst-case scenario earthquakes for Medellín (GSM, 1999).

## 2.2 ACCELEROGRAPH NETWORK DATA

Medellín is now the second most well instrumented city in Latin America, after Mexico City. The Medellín Accelerograph Network, R.A.M. (Red Accelerographica de Medellín), consists of 24 strong motion instruments recording motions at 22 different sites across the valley (see table 2.2). All but one of the instrument sites are located at one of 32 boreholes drilled as part of the microzonation study. The other station, ESE, is positioned on outcropping rock on the eastern hill high above Poblado and EAFIT University. Two of the sites (EET and POL) contain two instruments, one on the surface and one at depth. Both the ETNA and K2 surface accelerographs and the FBA-23DH borehole accelerometers record three components of motion (NS, EW, UD). These components are aligned to coincide with the orientation of the instruments within the National Accelerograph Network administered by the INGEOMINAS. Information is down-loaded to laptop computer on a regular basis. The accelerographs are housed inside a small masonry shelter close to the borehole (figure 2.2). The stations are mostly located within water reservoir enclosures, or the grounds of schools, colleges, universities and other public and private institutions, for reasons of security and power supply.

Some 27 earthquakes have been recorded between November 1996 and November 1999. On average, about 15 of the 24 instruments will be triggered during a small event. The records are

processed and archived at the R.A.M. Processing Centre within the Department of Civil Engineering at the Universidad EAFIT. Transfer functions and response spectra are calculated, and for events that trigger the instrument on bedrock (station ESE), Fourier spectral ratios (FSR) and response spectral ratios (RSR) are also computed with respect to motion at ESE (L.A. Palacio and J.D Jaramillo, pers comm.).

Station			Instrument		Altitude (m)	Bedrock Depth (m)	Geology
Location	Code	Borehole	Type	Depth			
Santa Elena Bedrock	ESE	-	ETNA	surface	2820	outcrop	SuM
Colegio Padre Manyanet	MAN	P-1	ETNA	surface	1605	46.90	KdA
Universidad de Medellín	UDM	P-2	ETNA	surface	1595	30.00	KdA
Sena sede Av, Colombia	SCE	P-3			1465	30.00	Qal
Sena Pedregal	SPE	P-4	ETNA	surface	1499	35.10	Qfm
Seminario Mayor	SEM	P-5	ETNA	surface	1877	48.00	KgD
Tanque El Tesoro	EET	P-6	K2	surface	1650	44.75	Qll
			FBA-23DH	10 metres	1640	34.75	Qfs
Comfama de Aranjuez	COM	P-7	ETNA	surface	1563	38.00	KuM
Centro de Control	ECC	P-8	ETNA	surface	1450	18.60	KPnl
Planta La Montaña	EMO	P-9	ETNA	surface	2170	19.50	KuM
F. Solidaridad Colombia	SOL	P-10	ETNA	surface	1660	22.90	Qc-Qat
Planta Villa Hermosa	EVH	P-11	ETNA	surface	1730	41.00	Qfm
Tanque Villa Tina	EVT	P-12	ETNA	surface	1822	28.55	KuM
Liceo Universidad	LIC	P-13	ETNA	surface	1688	38.55	Qff
Inspección San Joaquín	ISJ	P-14	ETNA	surface	1427	40.00	Qal
Tanque Aures	EAU	P-15	ETNA	surface	2026	20.00	Qfm
Facultad de Minas U.N.	FMI	P-16	ETNA	surface	1537	31.05	Qfm-Qat
Colegio San José	CSJ	P-17	ETNA	surface	1620	35.00	Qfm
Funación Amigo Policía	POL	P-18	K2	surface	1633	30.55	Qfm
			FBA-23DH	bedrock	1602	0.00	SdA
San Antonio de Prado	ITM	P-19	ETNA	surface	2048	29.85	Qf
Universidad Eafit	UEA	P-20	ETNA	surface	1518	18.00	Qal
Interconexión Eléctrica SA	ISA	P-21	ETNA	surface	1730	30.05	Qfs
Universidad Nacional	UNA	P-22	ETNA	surface	1488	15.90	Qal

Table 2.2. The Medellín Accelerograph Network (from GSM, 1999) the locations of these accelerographs within the Aburrá Valley are shown in figure 3.1 in the next chapter.

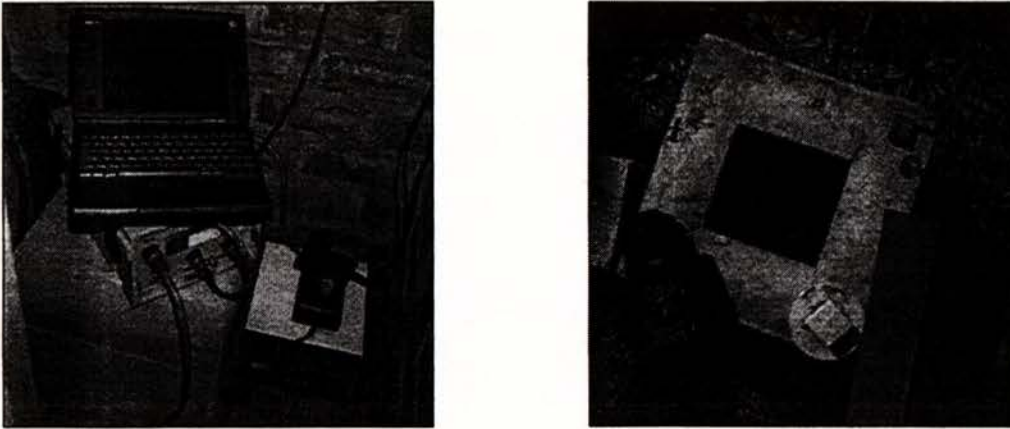


*Figure 2.2. Left: The seismograph and recorder at EET during downloading. Right: Borehole P-18 at POL. A cable descends the borehole to the FBA-23DH accelerograph at a depth of 30.5 metres.*

### 2.3 ABURRÁ VALLEY GEOLOGY

There are several different types of basement rocks in the area, all of which are plutonic (igneous rocks of intrusive origin) or metamorphic. The metamorphic rocks (gneiss and amphibolite) are the oldest and date back to the Cretaceous or possibly the lower Paleozoic, while the igneous stocks of dunite, gabbro, grano-diorite and diorite date back to the Cretaceous. There are several theories as to the origin of the deep Aburrá valley (see GSM, 1997 for a comprehensive compilation of various hypotheses). The idea that the valley may be a graben structure is most unlikely due to the compressive regime existing within the North Andes block (D. Rondón, pers. comm.). Almost certainly it is influenced by the north-south trending Romeral and Cauca fault systems of the western cordillera Central and Cauca valley, and possibly some form of extensional strike-slip duplex.

A variable depth of soft material exists above the basement rock within the valley. This soft covering may consist of one or any combination of (1) residual (weathered in-place) soils of the basement rocks, and (2) weathered non-consolidated alluvial and debris flow deposits dating back to the quaternary. These soft units may be anywhere up to 200 metres in depth (GSM, 1997), but are on average around 30 metres thick. The geomorphology of the land is in most cases highly correlated with the local geology. The steepest and most elevated parts of the city generally coincide with basement rock and/or a residual soil covering. The slopes characterised by moderate inclinations ( $\sim 10\text{-}30^\circ$ ) and elevations are often deposits of debris flows originating from higher and steeper slopes, while the flattest and lowest parts of the city are generally on alluvial deposits.

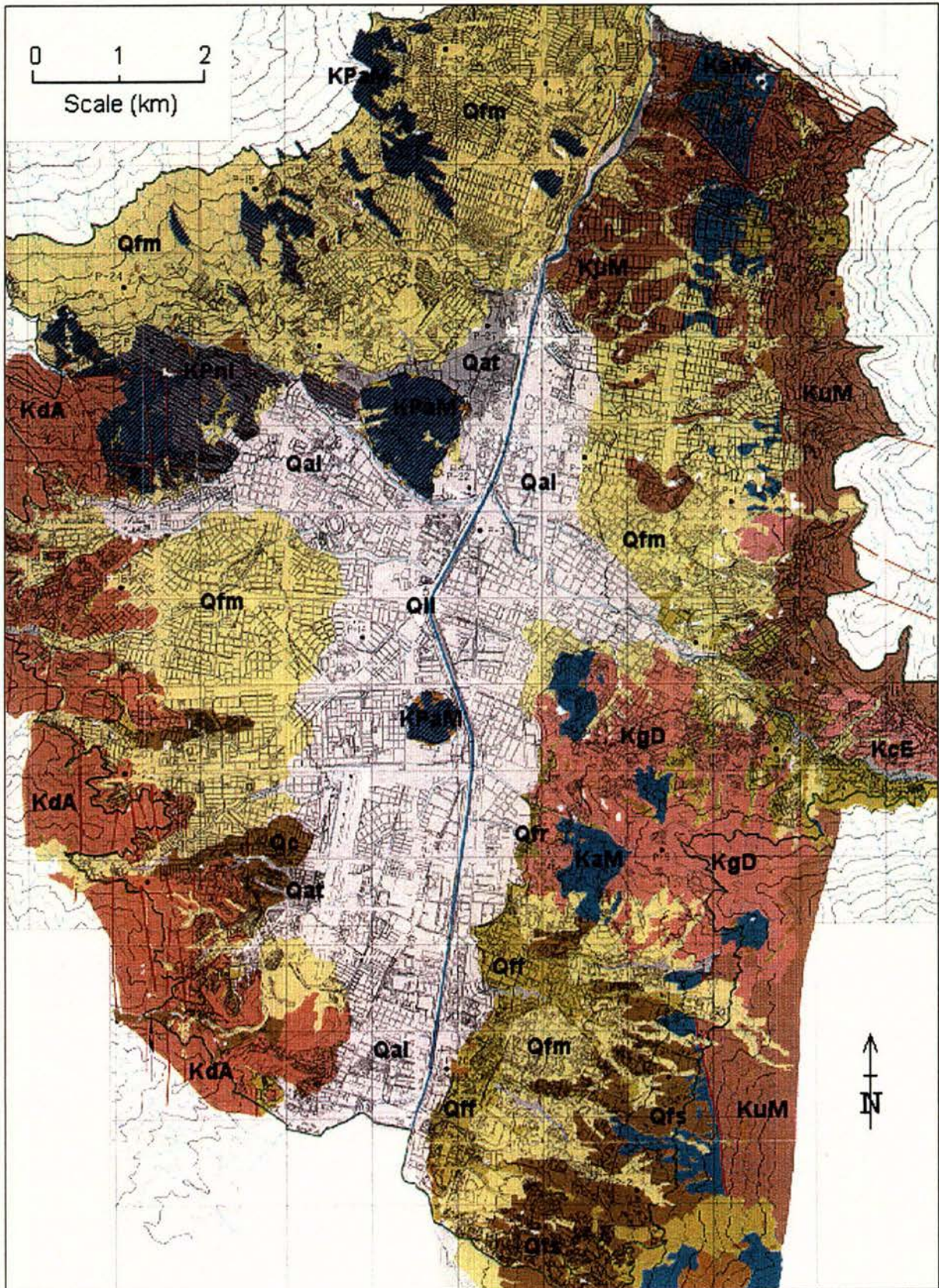


Figure 2.3. Geological map of Medellín (GSM, 1999). Table 2.3 provides a description of each geological unit.

Classification		Symbol	Name	Description
Basement Rocks	Metamorphic Rocks	SPnl	Iguaná Gneiss	Feldspar and quartz gneiss with clear foliation. Similar in texture and composition to a granodiorite (acidic plutonic rock).
		SPaM	Amphibolite West	Texture isotropic to banded and often similar to a gabro or diorite (mafic plutonic rocks). Hornblendes and Plagioclase dominant
		SaM	Amphibolite East	Gneiss-like texture with banding and well-formed lenses. Hornblende and plagioclase dominate over a small amount of quartz.
	Plutonic (Intrusive) Igneous Rocks	SuM	Medellín Dunite	An ultramafic intrusive rock with a colour between black, dark green and brown. Intensely fracturing exists in some parts of this unit.
		SgD	San Diego Stock	An intrusive body of mafic rock, mainly Gabbro with variations in composition and texture from phaneritic to pegmatitic.
		ScE	Las Estancias Stock	A small plutonic body of an acidic to intermediate rock (granodiorite) of phaneritic texture. Quartz and feldspar dominant.
		SdA	Altavista Stock	A large intermediate to mafic body (diorites and gabbros) whose composition and texture is very heterogeneous over the whole area.
Residual Soils	Weathered Metamorphic Rocks	KPnl	Iguaná Gneiss	Highly weathered. Well developed residual soil profiles with silts and clays of light colours between 15 and 40m thick.
		KPaM	Amphibolite East	Characterised by well developed residual soils grading from yellow-orange to grey-green silts. Generally between 20 and 30m thick.
		KaM	Amphibolite West	Generally weathered and well developed residual soil profiles of clayey silt between 15 and 30 metres thick.
	Weathered Plutonic (Intrusive) Igneous Rocks	KuM	Medellín Dunite	Soil between 10 and 40m thick depending on the competency of the original rock and the hydrological conditions etc.
		KgD	San Diego Stock	Well developed soil profiles upto more than 45m thick. Predominantly clayey silts.
		KcE	Las Estancias Stock	Strongly weathered, well developed residual soils between 30 and 35m thick. Sandy silts.
		KdA	Altavista Stock	Intensely weathered soil profiles that can reach 45m deep. Texture and grainsize depends on the parent rock.
Transported Deposits	Alluvial Deposits	Qal	Fluvial Deposits	Deposits of the Medellín river and smaller (Iguaná and Santa Helena) streams. Between 15 and 200 m deep. Pockets of clays, silts, sands, and coarse gravels. Horizontally variable yet normally graded.
		Qat	Flood Deposits	Heterogeneous deposits of all sizes. Contains a large quantity of blocks up to one metre in size and of diverse shapes. A chaotic mixture with a sandy silt matrix.
	Colluvial Deposits	Qc	Colluvial Deposits	A product of mass-movement on generally lower slopes. The composition depends on the origin of material. These deposits can reach more than 20m deep.
	Debris Flow Material	Qfs	Soil derived from Debris Flows	Easily confused with true residual soils of basement rock. Composed of a large number of highly weathered blocks embedded in a matrix of heterogeneous colour and texture.
		Qfm	Mature Debris Flows	Found lower down the hill than Qfs, forming a more moderate slope. Different sized blocks moderately to highly weathered, surrounded in a matrix similar to the material on the slope above.
		Qff	Fresh Debris Flows	Found lower still on the slope. Forms a smooth topography. Blocks of low to moderate weathering, surrounded by a generally wet and heterogeneous muddy matrix.
		Qfr	Recent Debris Flows	A product of the most recent events and hence found lowest on the slope. Angular and fresh blocks, composition depends on origin, surrounded by a loose, wet and brown sandy-silt matrix.
	Artificial Fill	Qll	Tropical Fills	Fills placed generally for construction purposes. Their composition is often extremely heterogeneous, consisting of both organic material and rubble.

Table 2.3. Geological units in Medellín (from GSM, 1999). The location of these units within the valley are shown on the geological map in figure 2.3.

The transported sediments, residual soils and basement rocks within the valley have been classified into several different geological units (GSM, 1997). Table 2.3 describes the main characteristics of each of unit. Here we briefly describe their spatial distribution within the valley, which is also shown on the contoured geological map in figure 2.3.

The oldest rock in the valley appears to be the Amphibolite (SPaM) of the eastern side of the valley. Both the Iguaná Gneiss (SPnl) and the Altavista Stock (SdA) have more recently intruded into the Amphibolite near the Iguaná stream. Residual soils covering the amphibolite (KPaM) and gneiss (KPnl) are up to 30 and 40 metres in thickness respectively.

Amphibolite (SaM) in the north-west flank of the valley is assumed to be separated from the Amphibolite on the east by some major (as yet undefined) tectonic structure along the line of the Medellín River. On the eastern side of the valley, the top of the Amphibolite is defined by a sub-horizontal contact with the Medellín Dunite (SuM) at about 1700-1900 metres amsl. The Medellín Dunite extends right along the eastern flank forming the top half of the hill. Figure 2.4 shows a profile through the residual soil of Medellín Dunite. Lower down on the western flank, there is intrusive contact between the Amphibolite and Gabbro of the San Diego Stock.



*Figure 2.4. Photograph showing a profile of residual soil of Medellín Dunite at a road cutting on the north-eastern flank of the valley. An interface between highly weathered soil and more competent rock can be seen sloping down to the right.*

The San Diego Stock (SgD) is a rhombic-shaped body of some 9km<sup>2</sup> in aerial extent, covering a large portion of the eastern flank south of the Santa Helena stream. Several fresh outcrops exist in road cuttings in the San Diego area. The residual soil profiles of San Diego Stock

(KgD) are perhaps deeper than any other rock, reaching more than 45 metres at station SEM. Las Estancias Stock (ScE) is much smaller and occupies an area of only 1.5-1.8 km<sup>2</sup> on the northern side of the Santa Helena Stream. Las Estancias Stock has intruded into the surrounding Medellín Dunite.

The Altavista Stock (SdA) extends over a large area on the western side of the valley south of the Iguaná Stream, where it forms an intrusive margin with the Amphibolite on the west. The south-west flank is characterised by very rugged topography above a large alluvial plain and sloping debris flow. The geomorphological classification (GSM, 1997) of these hills is given the name Unidad de cuchillas (Unit of large sharp knives!). The topography is one of very steep ridges bounded by steep canyons running westward toward the alluvial deposits of the Medellín River. Overlying the basement Altavista stock, is some 20-40 metres of residual soil (KdA).



*Figure 2.5. The terminal face of a debris flow from residual soils of Altavista forms an embankment to the left of the road in the lower south-west sector of the city.*

Debris flows mainly from the residual soils of Dunite, Amphibolite and Altavista Stock have created extensive areas of moderately sloping land at mid to low altitudes. They have been classified into four groups based mainly on the degree of weathering and location. The oldest flows (Q<sub>fm</sub>) are found both high on the slopes, and at the bottom of the stratigraphic column. Above these and lower down the slopes we find the more recent flows in order of occurrence (Q<sub>ff</sub> and Q<sub>fr</sub> respectively). On the south-eastern flank above Universidad EAFIT and Poblado, a significant portion of the oldest debris flows (Q<sub>fm</sub>) have undergone enough weathering to be able to be classified as a soil derived from debris flows (Q<sub>fs</sub>).

The Medellín river and other smaller streams (in particular the Santa Helena, La Iguaná and those from the Altavista in the south-west) have deposited a significant amount of alluvium (Qal) in the central and lowest part of the valley. As a result, the south-west sector contains the most extensive area of alluvial deposit between the debris flows and the Medellín River, some 1-2km wide. Topography on the alluvial deposits is smooth and the slope is generally less than 5%. The depth of this deposit has been found to be highly variable (between 3 and 200 metres). In the lower reaches of many of the side creeks, unsorted flood deposits (Qat) cover small areas. In several places, local mass-movements (up to 0.5km<sup>2</sup> in size) of various units have produced colluvial deposits (Qc) of various types. Finally, many small pockets of artificial fill (Qll) have been placed around the city, mainly as a result of construction operations.



*Figure 2.6. A construction gang removes a large boulder from an excavation into rubbly debris-flow deposits (Q<sub>fm</sub>) near accelerograph station POL (P-18).*

Several outcropping hills form noticeable irregularities in an otherwise smooth topography of the debris flows and alluvial deposits. The most interesting of these are a line of outcropping Amphibolite (SPaM-KPaM) peaks running in the NNE-SSW orientation on western side of the valley (figure 1.3). These are the prominent Cerro Nutibarra, Cerro Volador and Cerro El Picacho. Other less prominent hills include Cerro La Colinata (Altivista stock), Cerro Los Burgos (Gneiss), Cerro Santa Domingo Savio (Dunite), and Cerro El Salvador (Gabbro). These outcrops from a wide range of different rock types indicate that the basement is not necessarily very smooth or uniform. It is likely that, beneath both the debris flows and alluvial deposits which cover the majority of the urbanised part of the valley, the basement is highly irregular and capable of producing all manner of focussing and wave-path effects.

## 2.4 GEOLOGICAL AND GEOTECHNICAL DATA

The current database consists of information from a total of 940 boreholes drilled between 1955 and 1998, 32 of which were drilled as part of the most recent microzonation study. These 32 boreholes were located so as to obtain a representative sample of the different geology and geomorphology within the valley. They have an average depth of 29 metres, the deepest (48 metres) being located at station SEM and the shallowest (16 metres) at UNA (see table 2.2 and figure 3.1).

Borehole tests at the microzonation study sites and laboratory testing of intact samples have provided a large amount of geophysical and geotechnical data in addition to the stratigraphic information. This includes both static properties (density, plasticity, water content, grainsize distribution, penetration [SPT] values etc.) and dynamic properties (shear and compression wave velocities [ $V_S$  &  $V_P$ ], shear modulus [ $G$ ], fraction of critical damping [ $\beta$ ], and the variation of  $G$  and  $\beta$  with respect to strain from cyclic triaxial tests). These results have been compiled alongside surface geology observations, and subsequently integrated with a geographical information system (GIS) to produce a three-dimensional geological and geotechnical database of the city.

## Chapter 3: METHOD OF ANALYSIS

In this study we use both one-dimensional and two-dimensional finite-element methods to investigate the elastic seismic response of a typical cross-section through the Aburrá Valley. Fourier spectral ratios calculated by both these methods are then compared against those from recorded data at three different stations.

### 3.1 ABURRÁ VALLEY CROSS-SECTION AND TWO-DIMENSIONAL MODEL

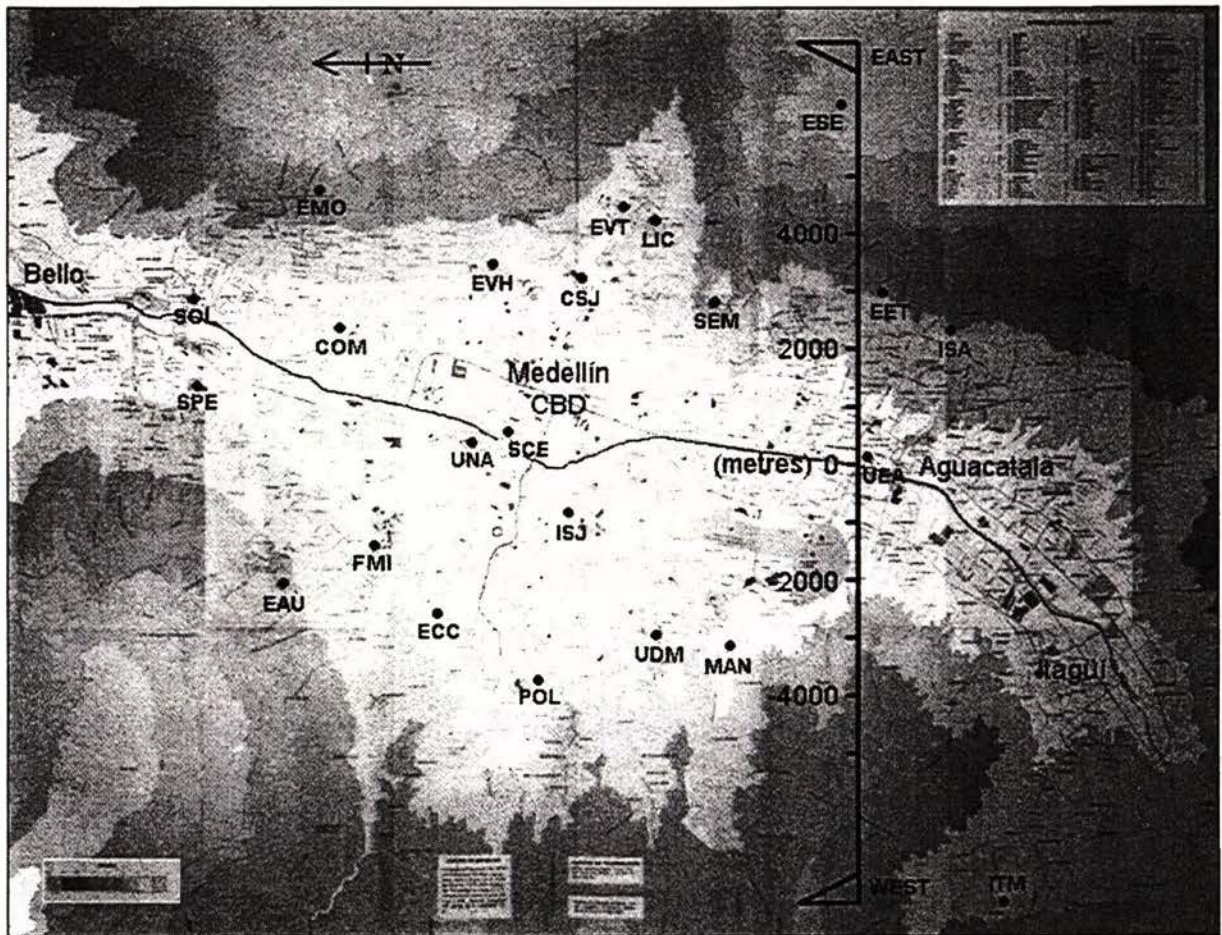


*Figure 3.1. Location of the cross-section through the Aburrá Valley, plotted on a relief map of Medellín showing shaded topographic contours (from Cartur, 1998). The location of the accelerograph stations are also shown (see table 2.2).*

In this study we take an east-west cross-section through the southern (upper) end of the city almost directly through the Universidad EAFIT. Here the valley is narrower and more two-dimensional than in the CBD, where the two major side streams (Iguaná and Santa Helena),

several hills (eg. Cerros Nutibara and Volador) and a leading ridge from the south-east dominate the topography (see figure 1.3). The geometry of the cross-section was taken directly from data in the 3-D geotechnical-geological model, geological maps and topographic maps (GSM, 1997) for a line with an orientation exactly east-west along the latitude  $6.204^{\circ}$  north (figure 3.1). At the upper end of the valley there is some 15km between the crests of the hills on either side. Figures 3.2 and 3.3 show the position of the cross-section on photographs of the southern end of Medellín.



*Figure 3.2. Photograph looking west across the valley from an altitude of approximately 2800 metres close to station ESE on the south-eastern hills. The line of the cross-section through the Universidad EAFIT cuts directly across the valley just to the right of the conveniently located tree.*



*Figure 3.3. Photograph looking south up the valley from Cerro Nutibara. The line of the cross-section through the Universidad EAFIT is indicated by the dashed black line. Note that this view is in reverse to the cross-section in figure 3.4.*

The cross-section in many ways typifies the topography and sub-surface geology of a 5km long section of the valley between Poblado, Aguacatala and Envigado. There is approximately 1-2km of reasonably flat alluvial plain to the west of the river and less than 0.5km to the east. The hills to the west of Aguacatala are part of the geomorphological sub-unit Cuchilla El Manzanillo, and reach an altitude of 2600 metres amsl. The slope is highly variable in gradient with many bumps and hollows. The average slope is in the order of  $8^\circ$ , while local inclinations may exceed  $20^\circ$ . The residual soil covering the Altavista bedrock to the west is between 20 and 40 metres deep. To the east, the crest of the hill lies at an altitude of 2820 metres. The sub-horizontal Dunite-Amphibolite interface lies at approximately 1850 metres amsl. Below this interface, both the Amphibolite bedrock and residual soil is covered by a significant thickness of debris flow deposits of various ages and weathering. Above the interface, the Medellín Dunite is covered only by a thin layer of residual soil.

The cross-section extends for 9320 metres either side of the Medellín River, giving a total model width of 18.64km. The lower semi-circular boundary of the model extends to a maximum depth of 1500 metres below the free surface in the centre of the valley. This boundary has a radius of 18,000 metres originating at the coordinates (0,18000). The inner boundary of elements where the excitation is input to the model has a radius of 16,800 metres. Using the mesh generator Triangle (Shewchuck, 1996) this geometry is used as the basis for constructing a fine mesh of triangular elements shown in the lower half of figure 3.4.

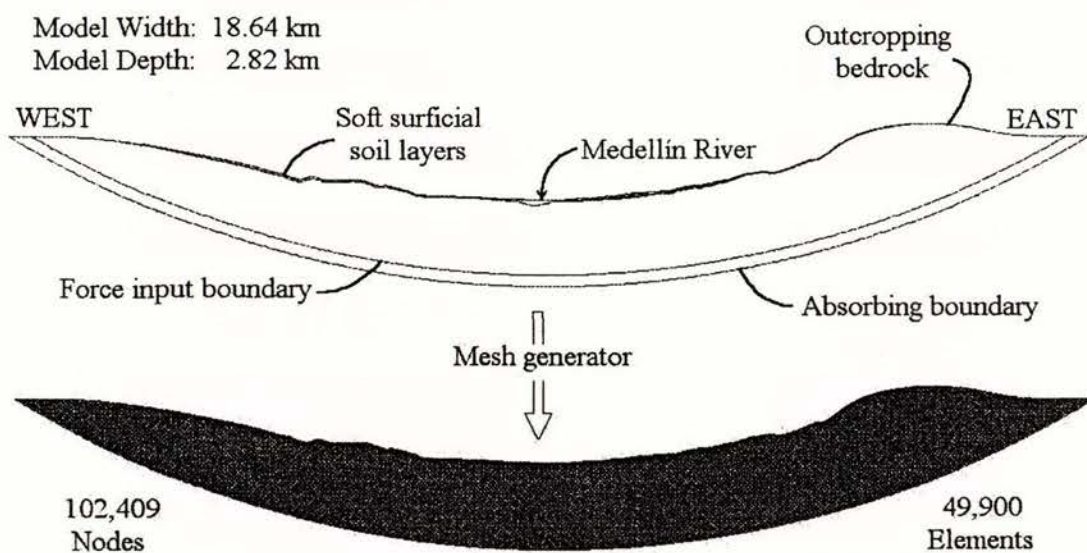


Figure 3.4. Geometry of the 2-D model through the Aburrá Valley. The 49,900 triangular elements in the lower plot are too small to be resolved at this scale.

## 3.1.1 GEOLOGICAL UNITS WITHIN THE MODEL

A total of twelve geological units are modelled; three different basement rocks, and nine different near-surface soft sediments. Of the soft sediments there are three residual soils, five naturally transported deposits, and a small deposit of artificial fill. Each of these units are given the geotechnical properties shown in table 3.1. Properties have been assigned on the basis of results from the comprehensive borehole and laboratory testing as part of the Medellín Instrumentation and Microzonation Project.

Both the soil and rock materials are assumed to be isotropic and homogeneous within each layer. In fact the real soils are highly anisotropic and inhomogeneous and are not so clearly defined into separate layers as the model assumes. Material properties within each layer may vary considerably both with depth and across their areal extent. Significant care has been used to make sure that the uniform properties assigned to each unit are representative of the variable reality.

Geological Unit		Bulk density $\rho$ (kg/m <sup>3</sup> )	S-wave Velocity $V_s$ (m/s)	Shear modulus $G$ (MPa)	Damping ratio $\zeta$ (%)	Poisson's ratio $\nu$	P-wave Velocity $V_p$ (m/s)	Lame's Constant $\lambda$ (MPa)	Elastic Modulus $E$ (MPa)
SaM	Amphibolite West	2650	2000	10,600	0	0.25	3464	10,600	26,500
SuM	Medellín Dunite	2650	2000	10,600	0	0.25	3464	10,600	26,500
SdA	Altavista Stock	2650	2000	10,600	0	0.25	3464	10,600	26,500
KaM	Amphibolite West Soil	1900	400	304	12	0.40	980	1,216	851
KuM	Medellín Dunite Soil	1900	350	233	8	0.40	857	931	652
KdA	Altavista Stock Soil	1700	250	106	4	0.40	612	425	298
Qal <sub>1</sub>	Alluvial Deposits Surf.	1500	150	34	7	0.45	497	304	98
Qal <sub>2</sub>	Alluvial Deposits Deep	1800	375	253	3	0.45	1244	2,278	734
Qfs	Soil of Debris Flows	1500	200	60	10	0.45	663	540	174
Qfm	Debris Flows Mature	1600	250	100	7	0.45	829	900	290
Qff	Debris Flows Fresh	1600	250	100	7	0.45	829	900	290
Qll	Artificial Fills	1500	150	34	7	0.48	765	810	100

Table 3.1. Elastic material properties of the twelve different geological units modelled in the cross-section.

## 3.1.2 NEAR-SURFACE STRATIGRAPHY

The soft near-surface sediments cover a 13.5km width of the model in the centre of the valley between -7325m and +6200m. The deposits have an average depth of 32 metres, and a

maximum depth of 94 metres. The central part of the valley contains a more complex succession of layering resulting from alluvial and debris flow deposition. The geometry of this area is shown by a series of four two-kilometre-wide plots in figure 3.5. In addition, figure 3.6 presents shows the non-structured finite-element meshes constructed for this same central 8km.

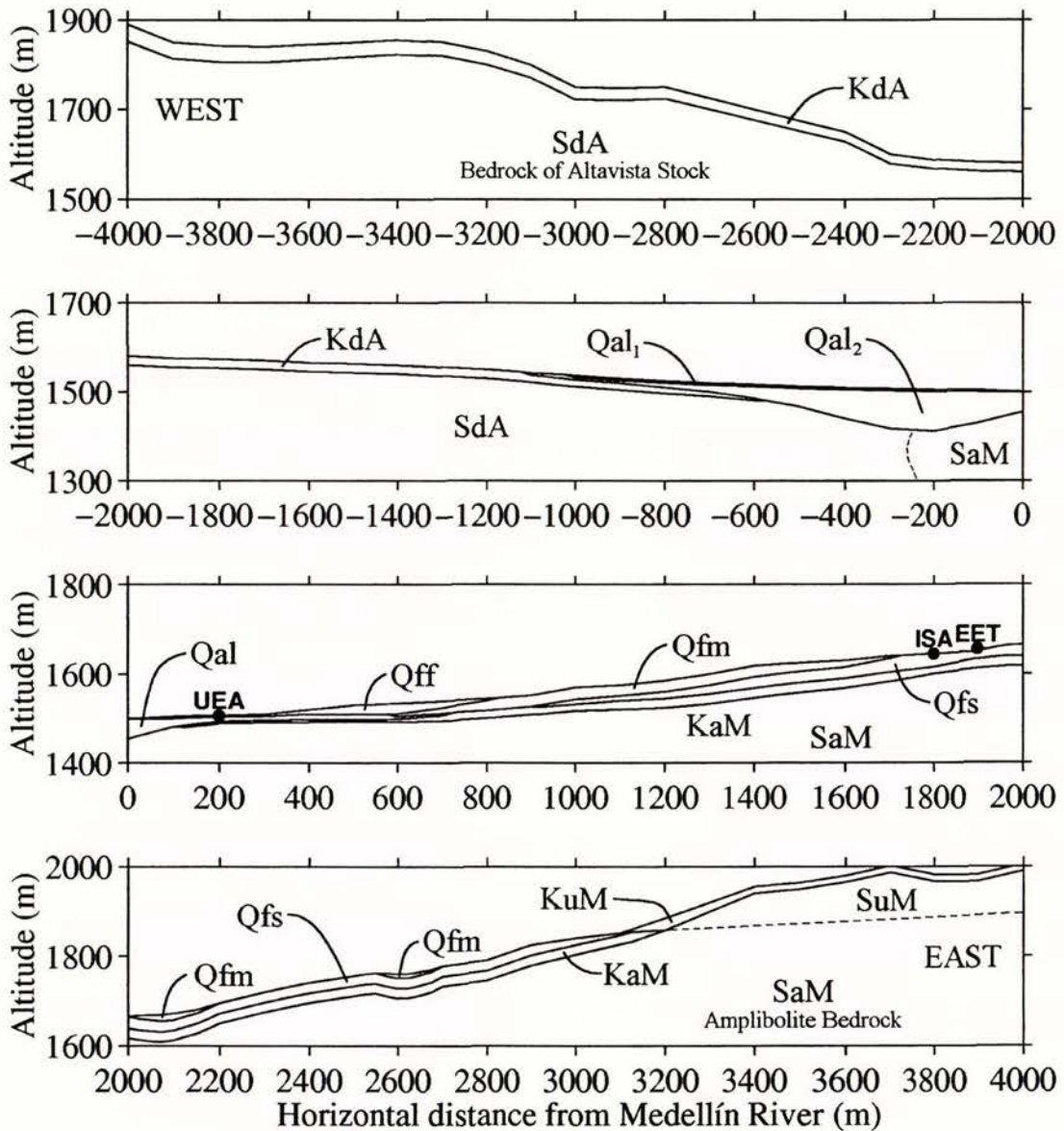
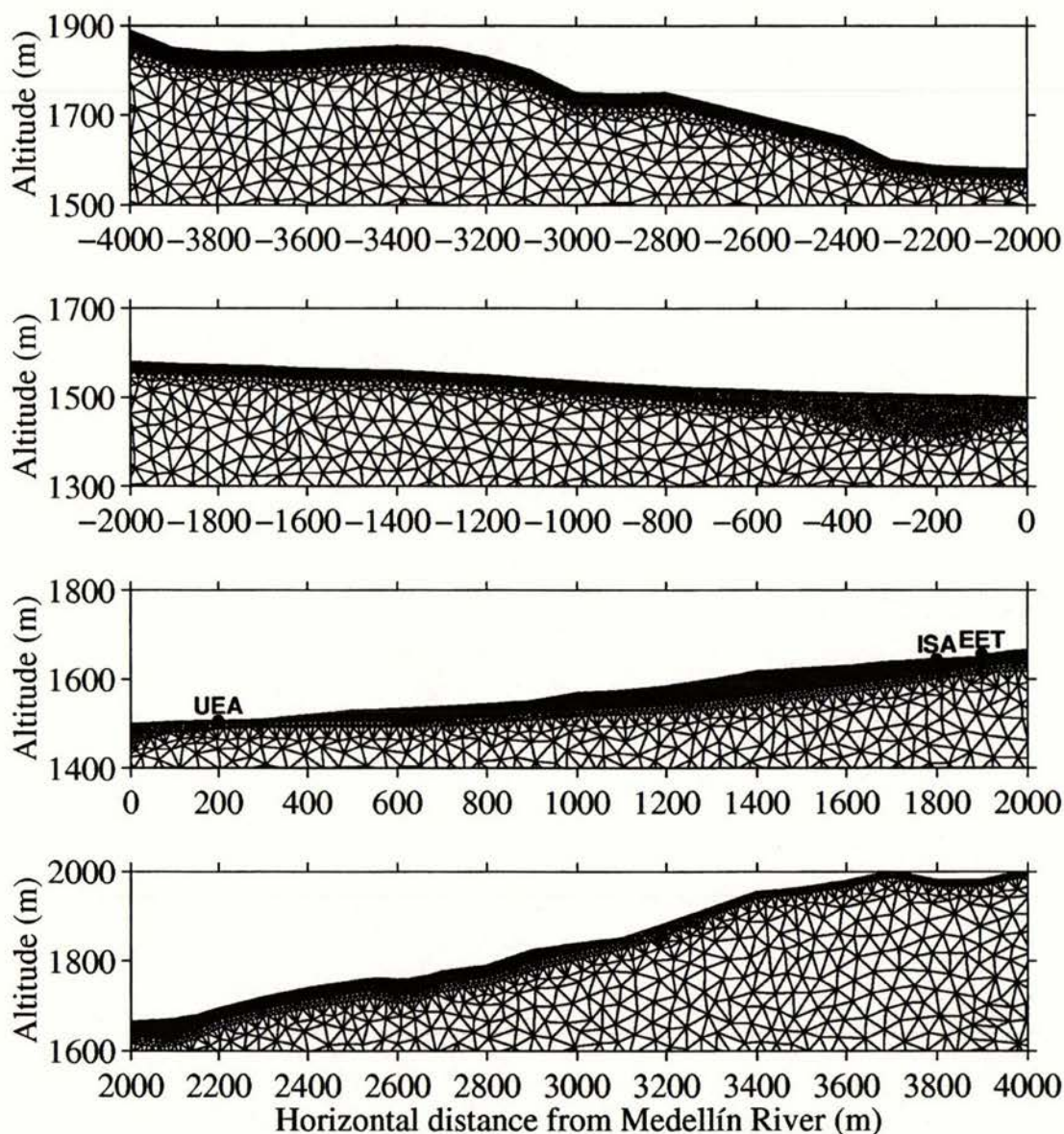


Figure 3.5. Showing the geometry of the various soft layers modelled across the central 8km of the cross-section. Each plot shows a 2km wide and 400m deep section of the surface of the model.

Finite element methods allow the use of an unstructured mesh, enabling elements of differing sizes and proportions to give a high degree of geometric detail. Node spacing can be tailored in proportion to the local shear-wave velocity to give similar numerical accuracy and high

computational efficiency throughout the geometry of the problem. The degree of geometrical detail we have used for the bedrock and sediment-layer boundaries is on par with the degree of certainty we have from existing geological data for Medellín. The cross-sections are defined by a set of linear segments between 2 and 100 metres in length along stratigraphic boundaries. Greater complexity could be incorporated if better quality geological data existed.



*Figure 3.6. Showing sections of the non-structured finite-element mesh across the surface of the model. Computational efficiency is achieved by tailoring the mesh size with respect to the minimum wavelength found in that layer (a function of the maximum frequency used in the modelling and the shear-wave velocity of the layer).*

In order to achieve high accuracy within the finite-element calculations, it is desirable to use a node spacing in the finite-element mesh of no greater than one-twelfth (Jacobo Bielak, pers.

comm.) of the shortest wavelength. Thus, since we use six-noded quadratic-triangular elements, with an intermediate node between each vertex, we have worked toward a maximum element size of one-sixth the minimum wavelength,  $\lambda_{\min}$ . In order to simulate seismic motions within the frequency range  $0 < f < f_{\max}$ , the corresponding maximum element size (the distance between vertices of the triangular elements) is required to be less than  $\lambda_{\min}/6$  (or  $V_S / 6f_{\max}$ ), where  $V_S$  is the shear-wave velocity of the unit. In this study we investigate frequencies up to a maximum of 5.0 hertz, and thus use elements between 5 metres (in soft alluvium,  $V_S = 150$  m/s) and 67 metres (in basement rock,  $V_S = 2000$  m/s) in size.

### 3.1.3 MODEL GEOMETRY AT THE ACCELEROGRAPH STATIONS

The line of the cross-section (figure 3.1) passes only 50 metres north of station UEA (P-20), 150 metres north of EET (P-6), and 1450 metres north of station ISA (P-21). It also passes very close to the position of station ESE on the rock outcrop on the eastern side of the valley. The stratigraphic data from each of the three borehole and accelerograph stations has been integrated into the model in order that we may compare results from recorded weak motions. With the centre of the Medellín River taken as the horizontal centre of the cross-section ( $x = 0$  metres) and the mean sea-level taken as zero in the vertical ( $y = 0$  metres), then within the cross-section the coordinates that typify the position of each of the accelerograph stations are shown in table 3.2.

Accelerograph station	horizontal (m)	altitude (m)
P-20 UEA	200	1507
P-21 ISA	1800	1645
P-6 EET	1900	1656
Rock Site ESE	6400	2820

Table 3.2. Accelerograph stations modelled within the cross-section.

Station UEA is located within the grounds of the Universidad EAFIT on the eastern side of the Medellín River. The borehole (P-20) at this location reaches competent bedrock at a depth of 18.0 metres (figure 3.7). This site lies above a shallow depth of alluvial sediments originating from the Medellín River and the nearby Aguacatala creek some 500 metres south. The top 3m of alluvial material ( $Qa_1$ ) has a much lower shear-wave velocity than the deeper gravels ( $Qa_2$ ). The topography around station UEA is very flat (figure 3.8). The Medellín

River lies 200m to the west, while the toe of the gently rising debris flows lie some 200m to the east.

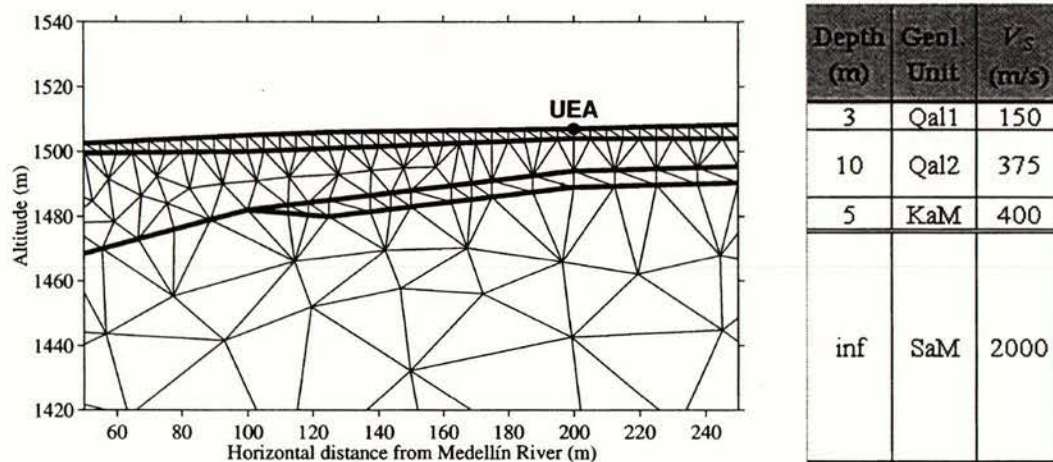


Figure 3.7. A section of the finite element mesh and a simplified borehole log modelling the geology beneath accelerograph station UEA (P-20).

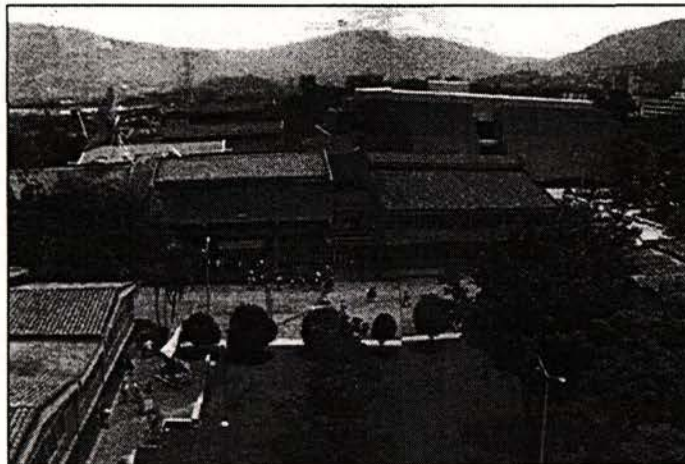


Figure 3.8. Photograph of Universidad EAFIT close to the site of the accelerograph UEA and borehole P-20. The topography is very flat.

Station ISA is located within the grounds of the electricity company Interconexión Eléctrica partway up the slope on the eastern side of the Medellín River. The borehole (P-21) at this location reaches competent bedrock at a depth of 45.0 metres (figure 3.9). The geology here appears to be relatively simple with a single deep layer of very weathered debris flow (Qfs) overlying 15m of residual amphibolite soil (KaM). The topography around station ISA is a gently rolling lumpy slope as shown in figure 3.10. The accelerograph hut appears to be situated on a 10m wide flat area perhaps cut into the side of the hill. Although this station lies over a kilometre south of the cross-section the geology and topography of both hill-slopes is very similar.

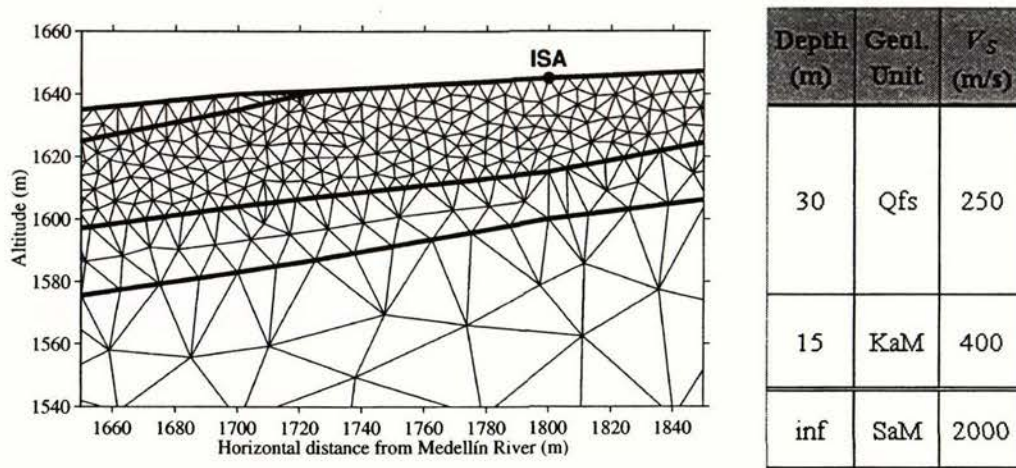


Figure 3.9. A section of the finite element mesh and a simplified borehole log modelling the geology beneath accelerograph station ISA (P-21).



Figure 3.10 Photograph of Station ISA and with the borehole (P-21) cover 2m to the left. The topography is gently rolling up to the right.

Station EET is located within the fenced-off grounds of a large municipal water storage tank (Tanque El Tesoro), midway up the slope of the eastern hills. The borehole (P-06) at this location reaches competent bedrock at a depth of 44.0 metres (figure 3.11). The accelerograph here lies on a shallow deposit of artificial fill above a depth of weathered debris flow material (Qfs) and residual soil of amphibolite (KaM).

The topography at station EET is very complex. The accelerograph hut and borehole are located on a small knoll of artificial fill as shown in figure 3.12. The artificial fill is likely to have been deposited during the excavation for the large water tank some 20 metres up-slope. Two metres downhill of the site there is a small bank perhaps 5 metres high. Five metres to the north a steep eroding cliff and sloping bank drops down into a ~15 metre deep gully and a small creek.

While the geological model (GSM, 1997) probably characterises this site adequately to a scale in the order of 50-100 metres, the complex topographic detail at EET is not shown. In an attempt to incorporate this detail into the two-dimensional model we have placed station EET on a small knoll of artificial fill (Qll) with a steep 6m high bank on the downhill side as shown in figure 3.11. The use of a two-dimensional approximation to characterise the geology and topography at EET is, however, perhaps far too simplistic.

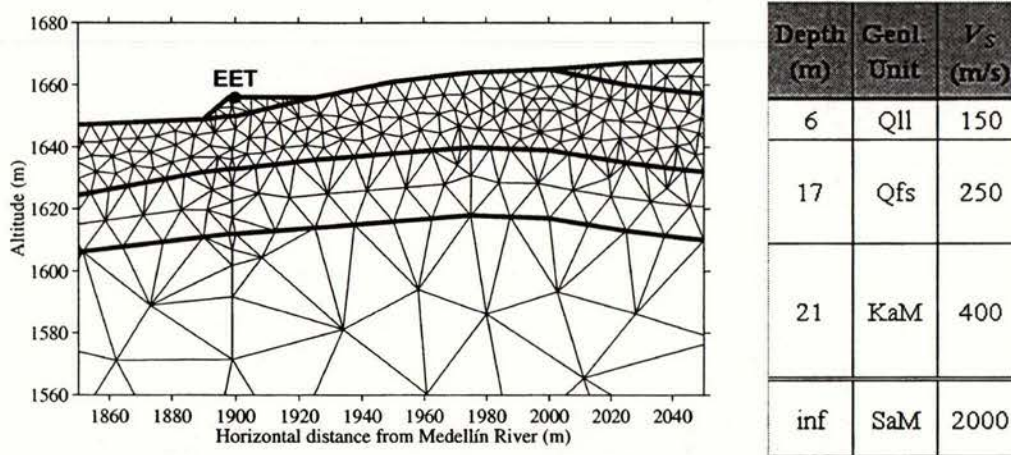


Figure 3.11. A section of the finite element mesh and a simplified borehole log modelling the geology beneath accelerograph station EET (P-06).

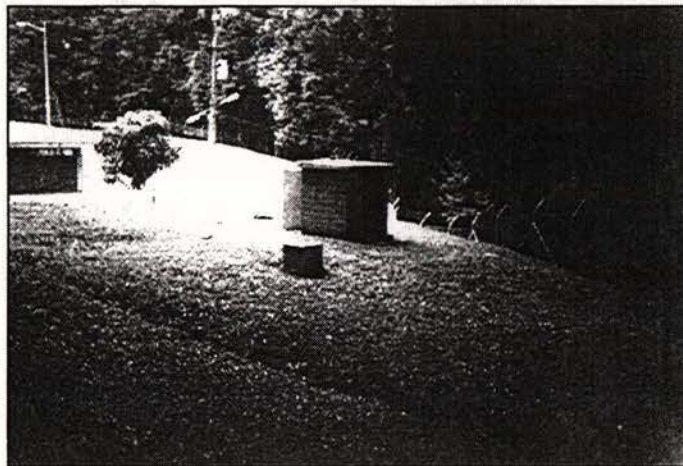


Figure 3.12. Photograph of accelerograph station EET with the borehole cover in front. The station is situated close to a large water tank and on a small knoll of artificial fill. Directly behind the photographer is a steep eroding cliff and a ~15 metre-deep gully.

### 3.2 TWO-DIMENSIONAL FINITE ELEMENT METHOD

To solve the problem of two-dimensional elastic wave propagation within our two-dimensional cross-section of the valley, we use a software package called Archimedes (Bao

et. al., 1998). Archimedes is an integrated set of computational software tools for performing large finite element method (FEM) simulations on parallel computers. It was originally developed for two-dimensional elastic simulations (eg. Bielak et. al., 1999, Adams et. al., 1999), while three-dimensional (eg. Hisada et. al., 1998) and non-linear techniques are now possible.

The software was developed as part of the National Science Foundation (NSF) Grand Challenge Quake Project, a joint venture between the Department of Civil and Environmental Engineering and the Department of Computer Science at Carnegie Mellon University (Pittsburgh, PA.), the Southern California Earthquake Center at the University of Southern California and the National University of Mexico. The Quake project has the goal of developing computer simulation methods for the prediction of ground motion in sedimentary basins during strong earthquake shaking.

Input to Archimedes includes (a) the geometry and properties of the geological model and (b) an FEM algorithm. The tool set, developed by Dave O'Hallaron and Jonathan Shewchuk of the Department of Computer Science at CMU, includes the following:

1. **Triangle** (Shewchuck, 1996) is a two-dimensional triangular mesh generator designed specifically for FEM's. It uses Delaunay triangulation algorithms to create an efficient, unstructured mesh. Input to Triangle includes the geometry of layer boundaries, free-surfaces and computational boundaries, maximum triangle area and minimum internal angle; all in the form of an ASCII data file (.poly extension). It also has the option of creating quadratic elements (six nodes per element) for more efficient computation. Output from Triangle consists of a set of three data files (.node, .ele, and .poly extensions) describing the coordinate points of each node and the nodes associated with each element. The 3-D equivalent, **Pyramid**, uses similar techniques to generate a three-dimensional unstructured tetrahedral mesh.
2. **Show Me** is a C program for graphically displaying on the screen meshes generated by Triangle. It also has functions for writing images to postscript files and for viewing the input geometry to Triangle.

3. A set of three programs - *Absorb*, *Slice* and *Parcel* - are used to refine, partition and reorganise the mesh data into a form that may be used on parallel processors. For our purposes, these programs were run with the input argument of only one processor. *Parcel* also requires an extra input file (with a .fi extension) containing five lines describing the input ricker-wave central frequency, the time-step size and the simulation length.
4. *Author* is the central tool of Archimedes. As input it uses data files (with extensions .adj, .def, .ele, .node, .pack, .part and .ri) from the previous tools, as well as an FEM code file (with a .arch extension) written in ANSI C and containing an element-level description of the finite-element approximation, and a high-level description of the finite-element algorithm. The job of *Author* is to compile these files into a processor code for running the simulation.

Up-to-date information and a description of the Archimedes tool chain may be found on the World Wide Web at <http://www.cs.cmu.edu/~quake/archimedes.html>. Complete documentation for the use of Archimedes has not yet been published, although complete instructions on the use of Triangle, the two-dimensional triangular mesh generator may be found at <http://www.cs.cmu.edu/~quake/triangle.html>.

### 3.2.1 THE FINITE ELEMENT ALGORITHM

In general terms, we are trying to solve the problem of elastic horizontally-polarised (SH) shear-wave propagation within a heterogeneous soft basin surrounded by a homogeneous half-space of rock. The half-space is idealised as of uniform cross-section and infinite-length (often called a cylindrical cross-section). We want to consider the effect of a transient anti-plane SH wave incident on this half-space. An FEM analysis allows us to treat the whole basin as piecewise uniform so that the displacement field,  $u$ , within each element, satisfies the wave equation

$$\frac{\partial^2 u}{\partial t^2} = V_s^2 \nabla^2 u \quad [3.1]$$

Boundary conditions are imposed which require the continuity of force and displacement across each element, and the absence of tractions at the free surface. The equation of motion

we wish to solve over the computational domain is a system of ordinary differential equations of the form

$$M\ddot{u} + C\dot{u} + Ku = f(t) \quad [3.2]$$

where  $M$ ,  $C$ , and  $K$  are the global mass, damping and stiffness matrices;  $u$ ,  $\dot{u}$  and  $\ddot{u}$  are the time-dependant nodal displacements, velocities and accelerations respectively, and  $f(t)$  is the applied nodal force

### 3.2.2 MATERIAL DAMPING

Damping has the effect of soaking up energy within the soil matrix thus inhibiting wave propagation. Likely values for the damping ratio,  $\zeta$ , have been assigned to each layer (see table 3.1) based on cyclic triaxial test of the various units (GSM, 1997). Archimedes uses a two-parameter ( $\alpha$  and  $\beta$ ) viscous Rayleigh damping model. Within each finite element, the damping matrix,  $C$ , has the form

$$C^e = \alpha\omega_o M^e + \frac{\beta}{\omega_o} K^e \quad [3.3]$$

where  $\alpha$  and  $\beta$  are arbitrary constants,  $\omega_o$  is a reference frequency, and  $M^e$  and  $K^e$  are the element mass and stiffness matrices. The Rayleigh damping model thus varies with frequency, so we select the  $\alpha$  and  $\beta$  parameters in such a way that the damping ratio averages out to the desired value across the frequency range of interest.

### 3.2.3 INPUT SIGNAL

The input motion is a single vertically propagating Ricker wavelet. In the time-domain, the displacement trace,  $u(t)$ , is given by (Ricker, 1940)

$$u(t) = A \left[ 1 - 2(\pi f_c t)^2 \right] e^{-(\pi f_c t)^2} \quad [3.4]$$

where  $f_c$  is the central (dominant or characteristic) frequency in cycles per second (Hertz) and  $A$  is the wavelet amplitude. In Archimedes, this same wave is approximated by

$$u(t) = \begin{cases} a_1(\omega_c t)^4 + a_2(\omega_c t)^6 + a_3(\omega_c t)^8 & 0 \leq t < \frac{\sqrt{6}}{\omega_c} \\ \left[ \frac{1}{4}(\omega_c t - 3\sqrt{6})^2 - 0.5 \right] e^{-\frac{1}{4}(\omega_c t - 3\sqrt{6})^2} - \frac{13e^{-13.5}}{0.5 + 13e^{-13.5}} & \frac{\sqrt{6}}{\omega_c} \leq t < \frac{5\sqrt{6}}{\omega_c} \\ a_1(\omega_c t - 6\sqrt{6})^4 + a_2(\omega_c t - 6\sqrt{6})^6 + a_3(\omega_c t - 6\sqrt{6})^8 & \frac{5\sqrt{6}}{\omega_c} \leq t < \frac{6\sqrt{6}}{\omega_c} \\ 0 & \text{elsewhere} \end{cases} \quad [3.5]$$

where  $\omega_c = 2\pi f_c$ , and  $a_1$ ,  $a_2$  and  $a_3$  are polynomial coefficients. Here the wavelet has been given finite start and finish points by substituting 3<sup>rd</sup> order polynomials at the start and end of the function. The peak displacement now occurs at  $3\sqrt{6}/(2\pi f_c)$  seconds. The Ricker waveform can be visualised in terms of its displacement trace,  $u(t)$ , and its Fourier amplitude spectrum as shown in figure 3.13. With a central frequency of 2 Hz, the Ricker pulse can be used to look at frequencies between  $\sim 0.1$  and  $\sim 5.0$  Hz.

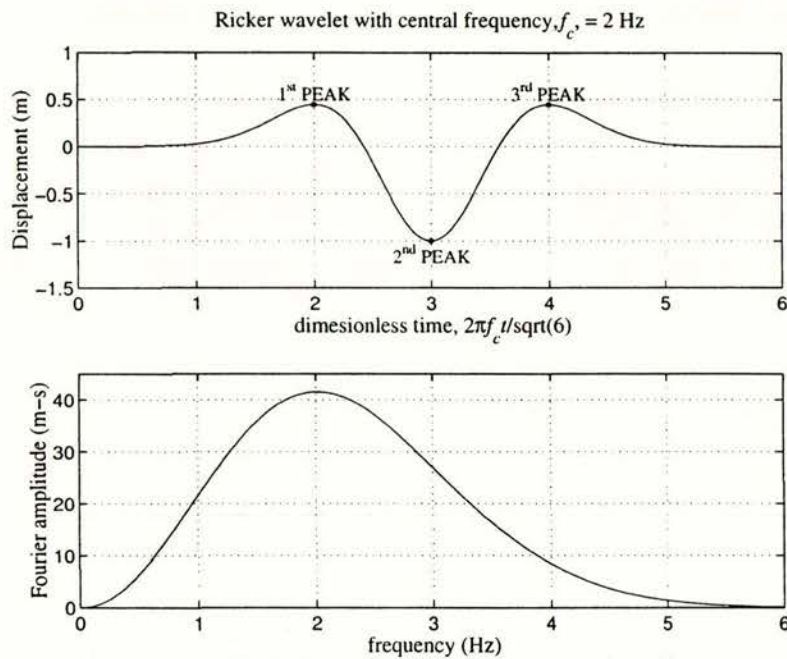


Figure 3.13. Plots of a Ricker wavelet in time domain and the corresponding Fourier amplitude spectra of displacement showing the central frequency and distribution of amplitude in the frequency domain.

The excitation is incorporated into the computational domain along a smaller semi-circular arc inside the absorbing boundary (see figure 3.4). The time of excitation of each node on the arc is adjusted so to represent a pulse starting simultaneously over the width of the mesh from the same depth. The method used is that developed by Bielak and Christiano (1984) and

Cremonini et. al. (1988) whereby nodal forces are applied along this inner arc of finite elements.

#### 3.2.4 *ABSORBING BOUNDARY*

Bedrock extends many kilometres below and to the sides, away from the soft basin. To keep memory requirements and calculation time to a minimum, we require a finite computational domain extending no more than a few hundred metres (several node spacings) into the rock. This introduces the problem of reflections from the artificial outer boundary, which need to be removed from the system. Al-Hunaidi (1989) describes and compares various solutions to this particular problem, one of which is the viscous boundary technique used here. A semi-circular absorbing boundary has been placed around the lower extent of the model, with the viscous boundary conditions, a distributed set of spring and dashpot models, imposed on the arc. The circular boundary has the advantage of being easy to describe mathematically as a singular bounding segment.

### 3.3 *ONE-DIMENSIONAL FINITE ELEMENT METHOD*

We use a short code written in MATLAB to calculate the time-domain response of an elastic SH wave travelling vertically within a column of homogeneous soil and rock units. The computation is in many ways very similar to that of the two-dimensional Archimedes code. The input excitation is again a Ricker wavelet as was shown in figure 3.13, while damping and the absorbing boundary are also incorporated in the same fashion to the two-dimensional method.

Using the same geometrical data and material properties that were used in the two-dimensional method, we are able to calculate the response to a Ricker wavelet at any point across the valley. The one-dimensional method requires that the waves be constrained to propagate in only one orientation (the vertical). In this way we rule out the possibility of focussing, surface-wave generation and other effects caused by non-horizontal geometry and of non-vertical wave incidence. The result we see for each given soil column is identical to that given by assuming a uniform stratigraphy extending to infinity in both horizontal directions, and bounded below by a uniform half-space.

### 3.4 POST-PROCESSING

Output from both the one-dimensional and two-dimensional finite-element analyses is in the form of displacement, velocity or acceleration time-histories of surface nodes across the width of the valley. From the two-dimensional simulations, we capture data from 581 surface nodes at spacings of between 10 and 50 metres. This is close enough to achieve good resolution for the identification of travelling surface waves. With the one-dimensional method we calculate the response for 201 soil columns across the valley. All calculations are carried out to 10 seconds (2000 time-steps using a step-interval of 0.005 seconds), which is generally sufficient to reduce the amplitude of wave oscillations back to nil.

A useful way to look at the effect of soft near-surface geology on seismic response in the frequency domain is with the Fourier Spectral Ratio (FSR). The FSR is defined (Borcherdt 1970) as the ratio of the Fourier amplitude from a recording on the *soil surface* to the Fourier amplitude from a simultaneous recording on a *bedrock outcrop*,

$$FSR(\omega) = \frac{|F_{soil\ surface}(i\omega)|}{|F_{rock\ outcrop}(i\omega)|} \quad [4.6]$$

where  $\omega$  is the frequency,  $F_{soil\ surface}(i\omega)$  is the complex Fourier transform of the output seismogram at the soil surface and  $F_{rock\ outcrop}(i\omega)$  is the Fourier transform of the output on a rock outcrop. All phase information is lost in the calculation of the FSR. The purpose of the FSR is to cancel out the effect of the input motion and reduce the results to show only the effect of the soft near-surface geology. Thus, in theory, the results should be earthquake-independent, and a function only of the surface layers.

For the case of a uniform half-space of perfectly elastic rock, the outcrop surface motion (ie. the output from the simulation) is expected to have twice the amplitude of the bedrock basement motion (ie. the input to the simulation). The actual response from the numerical computer simulations is slightly erratic, although of similar amplitude and shape to the analytical solution. Thus to obtain a smoother FSR from model results, it is calculated directly from the input motion,

$$FSR(\omega) = \frac{|F_{o,surface}(i\omega)|}{2|F_{i,bedrock}(i\omega)|} \quad [4.7]$$
$$FSR(\omega) = \frac{1}{2}|H(i\omega)|$$

where, the subscripts  $i$  and  $o$  refer to input and output respectively and  $H(i\omega)$  is the complex transfer function between the basement and the surface.

Both displacement time-histories and FSR's at each evenly spaced position across the valley can be plotted close together on position-time or position-frequency axes, with amplitude shown as a colour scale. These plots show clearly patterns of amplification as a function of position within the Aburrá Valley.



---

## Chapter 4: RESULTS

---

Results are presented here from one-dimensional and two-dimensional finite element analyses, and they are compared in both the time and frequency domains. Fourier spectral ratios from the numerical analyses are then plotted against recorded data at three accelerograph stations. The results and implications thereof are then discussed in the following chapter.

### 4.1 TIME-DOMAIN ANALYSIS

Figures 4.1 and 4.2 show displacement seismograms computed across the surface of the Aburrá Valley by two- and one-dimensional analyses, respectively. The output shown is the displacement due to the input of a vertically propagating SH Ricker wavelet with a central frequency,  $f_c$ , of 2.0 Hertz (figure 3.13).

#### 4.1.1 AMPLIFICATION OF THE FIRST ARRIVAL

The plot in figure 4.1 shows an amplified first arrival of the vertically propagating wavefront. The left-hand-most dark-blue line shows the first (positive) peak of the Ricker displacement pulse arriving at the surface across the full width of the valley. The central (negative) peak of the wavelet arrives a short time later and is plotted green-yellow-orange, while the third (positive) peak is again dark-blue going purple. This wavefront is variably amplified and arrives at different times depending on both the altitude and shape of the topography, and the depth, geometry and material properties of any soft layers beneath.

The initial arrivals calculated by the one-dimensional and two-dimensional analyses are compared in figure 4.3. A separate axis is used for each of the three peaks of the Ricker wavelet. Each plot shows the surface displacement normalised against the input displacement of that peak. In the rock outcrops on each side of the model, each peak has been amplified by a factor of two. This is free-surface doubling. Within the part of the valley that is overlain by one or more soft layers, the amplification is much higher. The stratigraphy and depth of these soil layers is shown on the right of the figure. They extend from  $-7325\text{m}$  to  $+6200\text{m}$ .



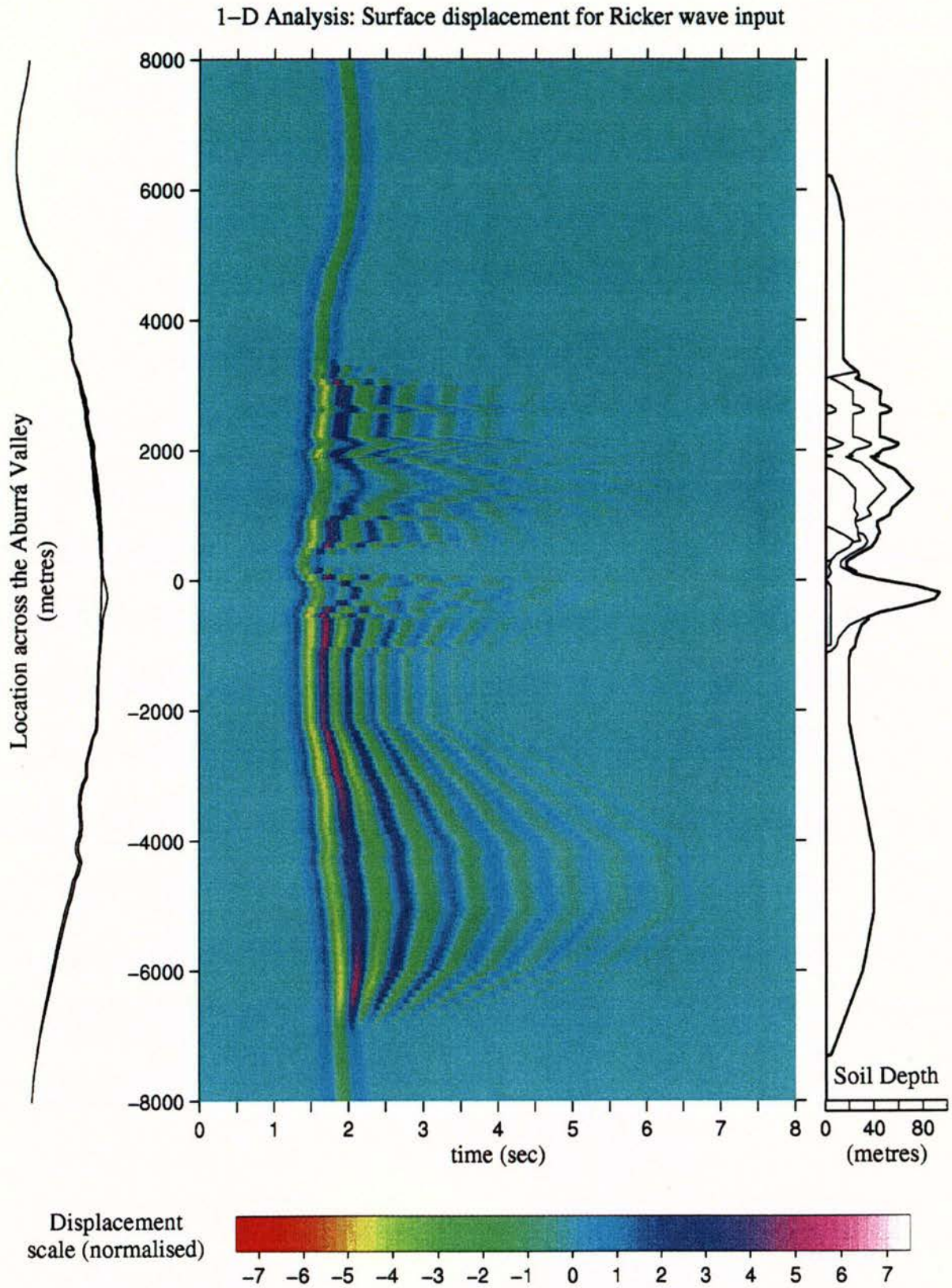


Figure 4.2. Displacement time-histories at the surface from the one-dimensional FEM analysis of two hundred points across the valley. Normalised displacement amplitude is shown as a colour scale. The plot of sediment depths shown on the right-hand axis represents the geometrical model used in analysis.

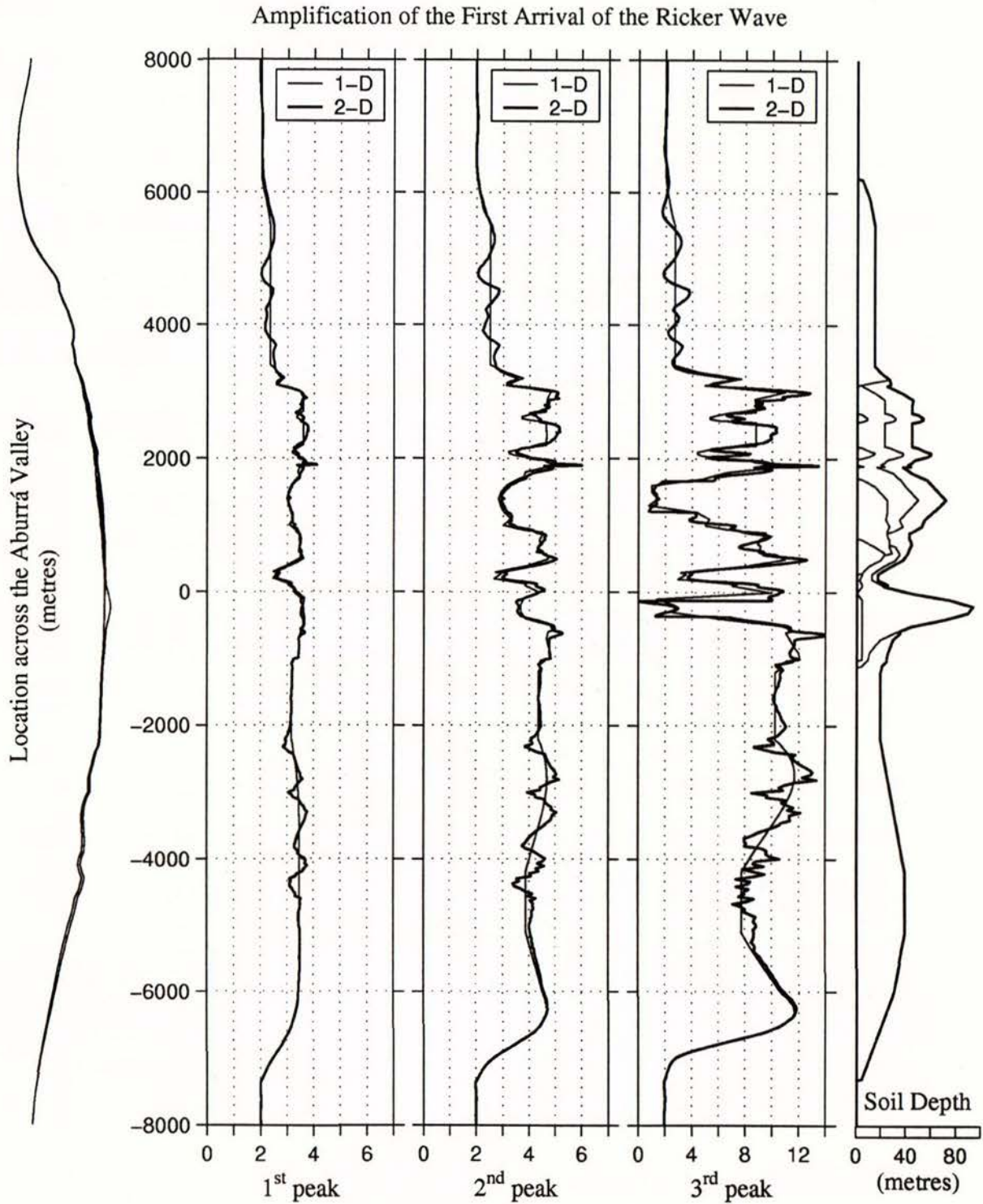


Figure 4.3. Plots showing the amplitude of the three different peaks of the Ricker wavelet (figure 3.13) when it first arrives at the surface. Results from both one-dimensional and two-dimensional analyses are shown. Displacement for each of the three peaks is normalised against the input wavelet, such that in the rock at the edges, the value of two indicates free surface doubling.

One-dimensional and two-dimensional results compared in figure 4.3 are in general similar. The 1-D result is, however, much smoother and visibly a function only of the stratigraphic depths and properties, whereas local deviations of the 2-D result from the 1-D result can be seen across the width of the sediments. These deviations indicate the action of two-dimensional amplification within the model. The mechanisms for the amplification of these peaks of first arrival are most probably focussing due to the geometry of the soft layers, and focussing due to the geometry of the topography.

Amplification of the second and third peaks in the initial surface arrival are significantly larger than the first. Two-dimensional effects (indicated by the deviation of the 2-D result from the 1-D) are also stronger in the arrivals of the second and third peaks. This is perhaps a result of additional scattering caused by interaction between the down-going and up-going waves.

#### 4.1.2 *SURFACE WAVE ACTION*

In figure 4.1, there appears to be little evidence of surface wave action generated by the 2-D analysis. This is especially noticeable when compared to similar analyses of narrower basins with deep sediments such as the Lower Hutt (Adams et. al., 1999), where strong surface waves are generated at each edge of the valley. Weak surface waves, however, appear to be generated from small anomalies in the topography at 3800m and 5400m on the east. They are shown on figure 4.1 as diagonal lines originating from the initial wavefront. Weak surface waves are also generated at the edges of the deep alluvial dip in the centre of the plot, and at the edges of the next-thickest layer of sediments between +1000 and +1800m. The former pair of surface waves cause amplification where they interfere constructively at -250m. On the whole, this model does not appear to be strongly effected by the presence of surface waves.

#### 4.1.3 *VERTICAL WAVE REFLECTION AND RESONANCE WITHIN THE SOFT LAYERS*

In some parts of the valley, the SH wave appears to reflect up and down within the soft surface layers more strongly than at other locations. This can be seen on figures 4.1 and 4.2 as a repeated pattern of wavefronts reaching the surface in a fashion that extends or stretches the shape of the initial arrival. In the 1-D analysis these oscillations at the surface decay to

insignificant amplitude after only 4-5 cycles of reflection. In the 2-D results, however, the oscillations continue for up to 12 or more cycles, and they also stretch the shape of the initial arrival in a much more complex manner. In general, oscillations continue for the longest in the regions of thickest sediments. This result, however, is highly dependent on the dominant frequency of the input wavelet. For this reason we see no oscillations west of 3000 metres, where the bedrock is overlain by a single thin layer of residual soil of Medellín Dunite. The wavelength of the Ricker pulse is too long compared to the layer thickness for it to be trapped and cause vertical resonance.

#### 4.1.4 *ERRORS DUE TO INCOMPLETE ABSORPTION AT THE ARTIFICIAL BOUNDARY*

In the two-dimensional result shown in figure 4.1, on the eastern 5000 metres of the plot (from +3000m to +8000m), we see an additional line of branching wavefronts reach the surface 3-4 seconds into the simulation. These waves are an unfortunate scattered reflection from the lower artificial boundary, and subsequent scattering from the free surface. They are the product of an inexact numerical calculation. The spring and dashpot boundaries require a plane free surface and a uniform half-space to work perfectly and remove all out-going waves in the model.

In the case of the Aburrá Valley, large-scale topography has contributed enormously to the degree of wave scattering and subsequent inefficiency of the artificial boundary. The dark-blue peak at 5000-6000m and ~3.7 seconds is a result of focussing of the absorbing boundary reflections due to the shape and position of both the absorbing boundary and the free surface. The reflected wavefronts from the absorbing boundary are highest between +3000m and +8000m due to the lack of soil covering, or only a thin covering of stiff soil (KuM). This lack of a deep soft layer causes the bulk of the input energy being reflected back down into the half-space for removal by the absorbing boundary. The highly scattered nature of the wave renders the absorbing boundary reasonably inefficient in this case.

We can also see evidence of this numerical inaccuracy across the rest of the basin, especially where it constructs with validly scattered waves within the model. This mechanism appears to be the cause of the erroneously high (purple and yellow) peaks at -6200m and -4700m in the 3-4 second range.

#### 4.1.5 *TRANSIENT RESPONSE IN THE REGION OF THE ACCELEROGRAPH STATIONS*

The three accelerograph stations modelled in the study lie within the width of valley covered by more than one layer of soft soil, that is, between  $-1500\text{m}$  and  $+3500\text{m}$ . The two-dimensional transient displacement response for this section of the valley is shown in figure 4.4 (an expansion of figure 4.1), while the peaks of the initial arrivals are shown in figure 4.5 (an expansion of figure 4.3). The main features of the response in this area are described here from west to east. The calculated transient response at the stations UEA, ISA and EET are shown in figure 4.6.

On the western edge of the large alluvial dip, between  $-700\text{m}$  and  $-600\text{m}$ , the amplification of peaks of the first arrival (best viewed on figure 4.5) are significantly higher in the 2-D analysis. This appears to be some form of edge effect either in the residual soil (KdA) extending west from this point, or in the alluvial dip to the east. Within the alluvial dip ( $-600\text{m}$  to  $+100\text{m}$ ) surface waves are clearly visible, being generated at the edges by the first arrival and travelling back and forth across the small basin for several cycles. The amplitude of these waves is much reduced after the first crossing of the alluvium due to its poorly defined edge (as it grades into adjacent thinner layers) with correspondingly poor horizontal reflection characteristics.

At the site of station UEA, only 100 metres east of this alluvial dip, we see little evidence of the weak the basin effect. In figure 4.6, amplifications of the first arrival are slightly higher from the 2-D analysis. The majority of the later small oscillations appear to be a result of the numerical inaccuracies described in section 4.1.4. Although this position in the model is characterised reasonably well by the 1-D analysis, there is still evidence of minor multi-dimensional effects.

Between stations UEA ( $+200\text{m}$ ) and ISA ( $+1800\text{m}$ ) the 2-D analysis produces many local deviations from the 1-D amplification of the first arrival shown in figure 4.5, yet the general trend is very one-dimensional. On figure 4.4, however, weak surface waves appear to travel across the sediments with the effect of lengthening the increasing the number of oscillations in the 2-D result.

At the position of station ISA, the peaks in figure 4.6 are amplified more in the 2-D result and the oscillations continue for longer. At station EET, the 2-D peaks are amplified significantly

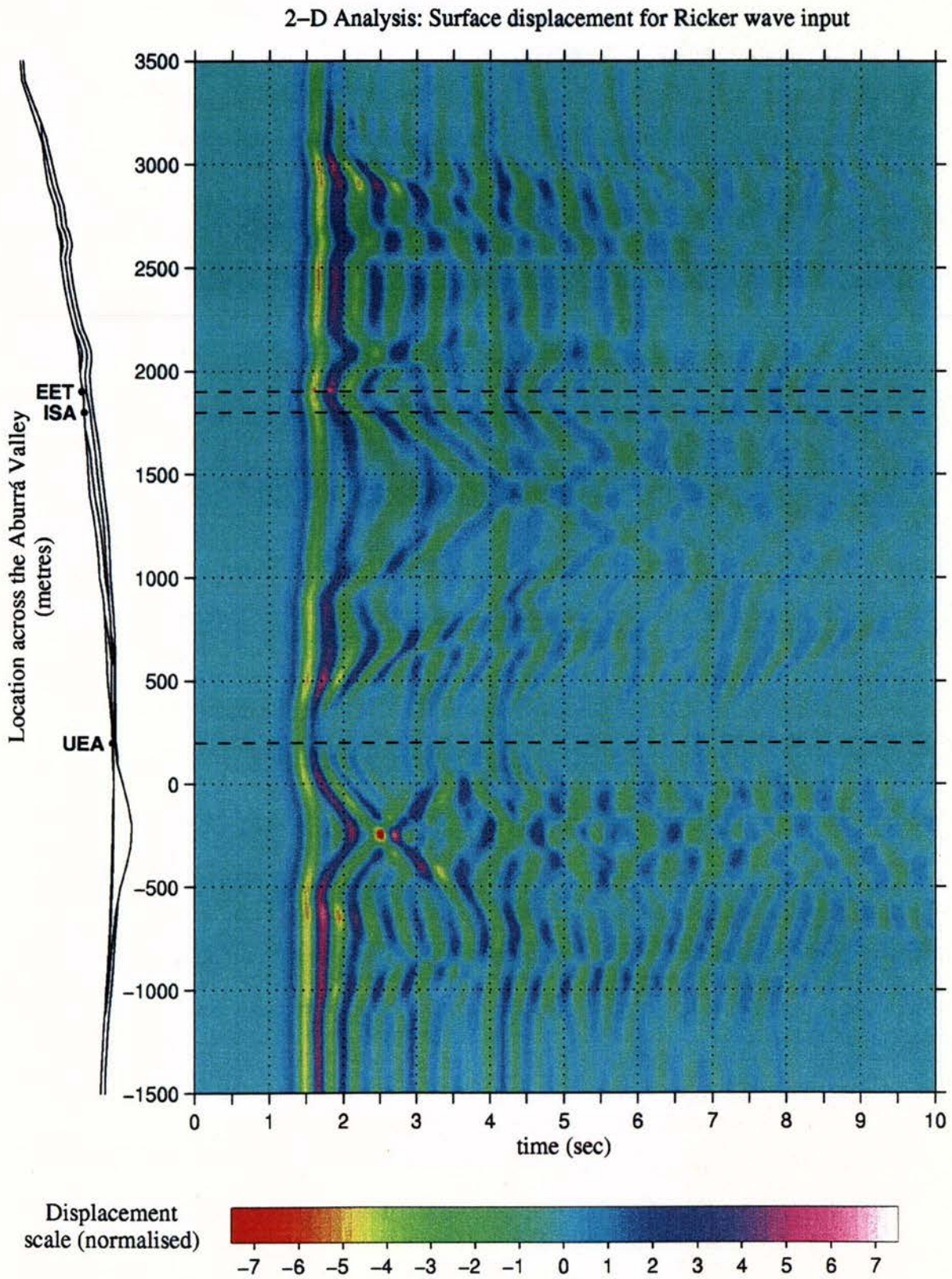


Figure 4.4. An expansion of figure 4.1 for the central-east 5km of valley, showing the locations of accelerograph stations UEA, ISA and EET.

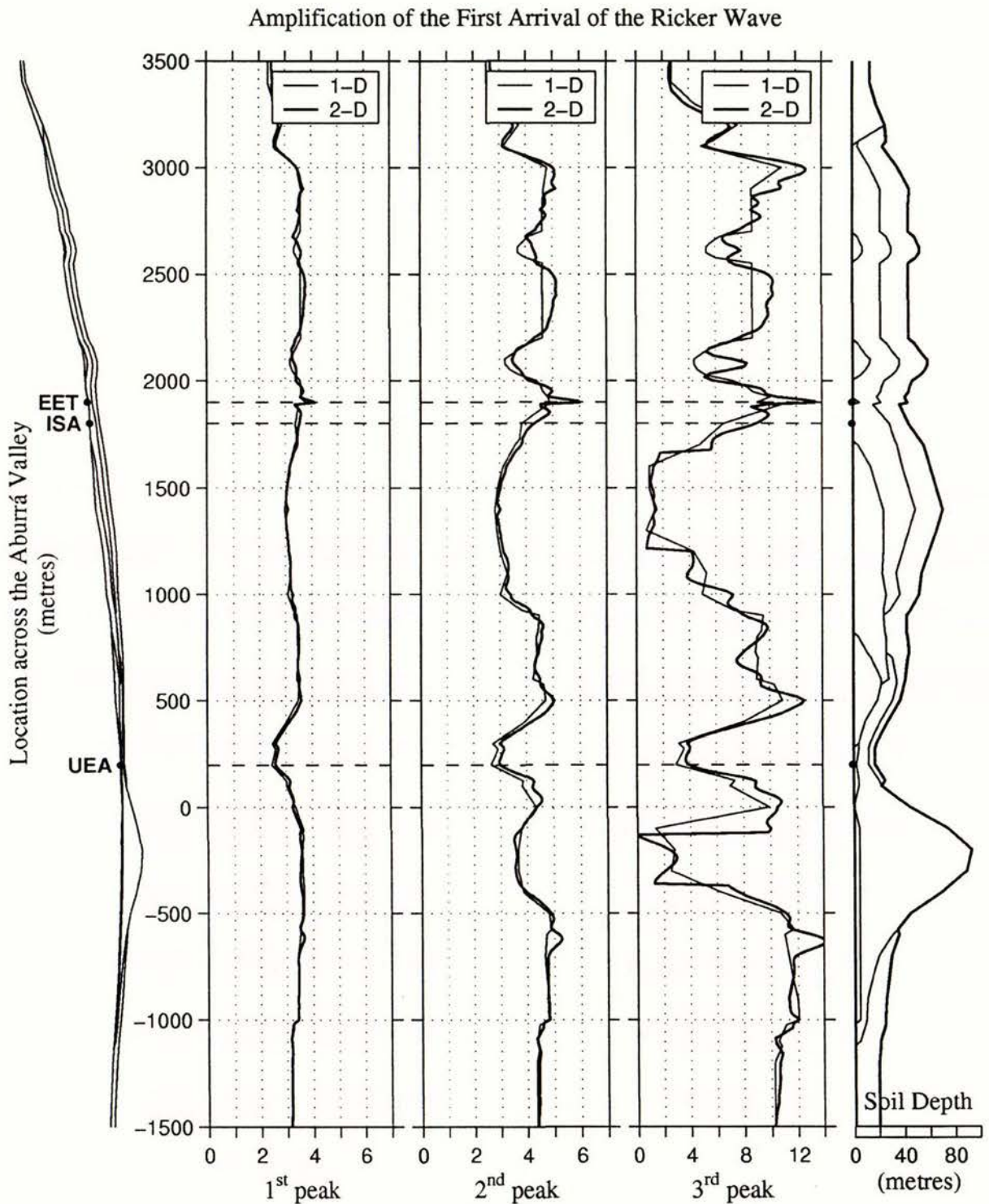


Figure 4.5. An expansion of figure 4.3 for the central-east 5km of the valley, showing the locations of accelerograph stations UEA, ISA and EET. Sediment depth plotted on the right of the figure correlates well with peak displacement from both the one-dimensional and two-dimensional analyses.

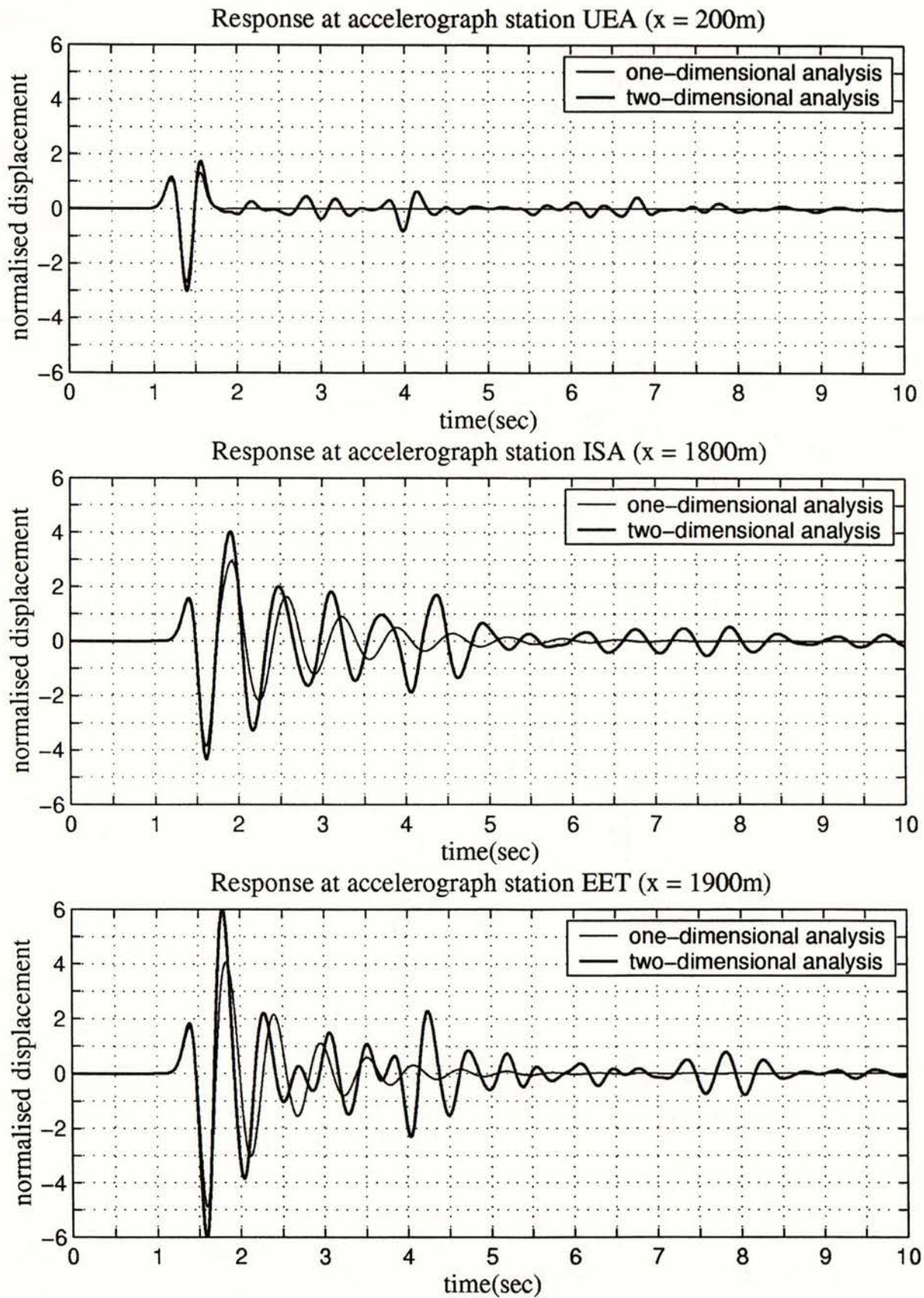


Figure 4.6. Displacement time-histories at accelerograph stations UEA, ISA and EET for a Ricker wave input. One-dimensional and two-dimensional results are compared.

more than the 1-D (50% more for the 3<sup>rd</sup> peak). This is clearly seen on both figures 4.5 and 4.6. The shape of the displacement trace at EET in figure 4.6 is also very different, and the shaking more prolonged. Again the peaks at 3 and 4 seconds have undoubtedly been influenced by the numerical reflections described in section 4.1.4. It appears that two-dimensional effects at EET are a result of both the protruding knoll of artificial fill (figure 3.11) and the deeper soft layers also found at ISA.

## 4.2 SPECTRAL ANALYSIS

Figures 4.7 and 4.8 show plots of Fourier spectral ratio (FSR) computed across the surface of the Aburrá Valley by two- and one-dimensional analyses, respectively. On the rock outcrops to either side of the valley, the FSR has an approximate value of unity (a red colour on both plots) for all frequencies, as expected. Within the part of the valley covered by soft soil, however, a complex pattern of amplification exists.

### 4.2.1 A COMPARISON BETWEEN ONE- AND TWO-DIMENSIONAL ANALYSES

The 1-D result in figure 4.8 appears to correctly predict the approximate position of the main peaks in the 2-D result (figure 4.7), yet it does not reproduce any of the very high FSR values nor the spatial variability thereof. FSR in the 1-D results reach a maximum of 8.7 between –5000m and –4000m, and the spectral amplification is generally quite uniform across the whole valley with an average peak FSR of around 7 (a green colour on figure 4.8). The frequency at which this peak occurs is a simple function of the depth and properties of the layers below.

In the 2-D results the FSR peaks at more than 18 at several locations. In most cases, the frequency at which peak amplification occurs is very similar to the 1-D prediction. The strong spatial variability and amplification shown in figure 4.7 is clear evidence of two dimensional effects, such as focussing, surface wave action and horizontal resonance. These appear to occur over the whole of the soft part of the valley.

In addition to the large peaks in the results on figure 4.7, there exists a background low-amplitude valley-wide spectral pattern. This is viewed as the curved yellow lines most noticeably on the eastern (top) portion of the plot. These lines are not observed in the results

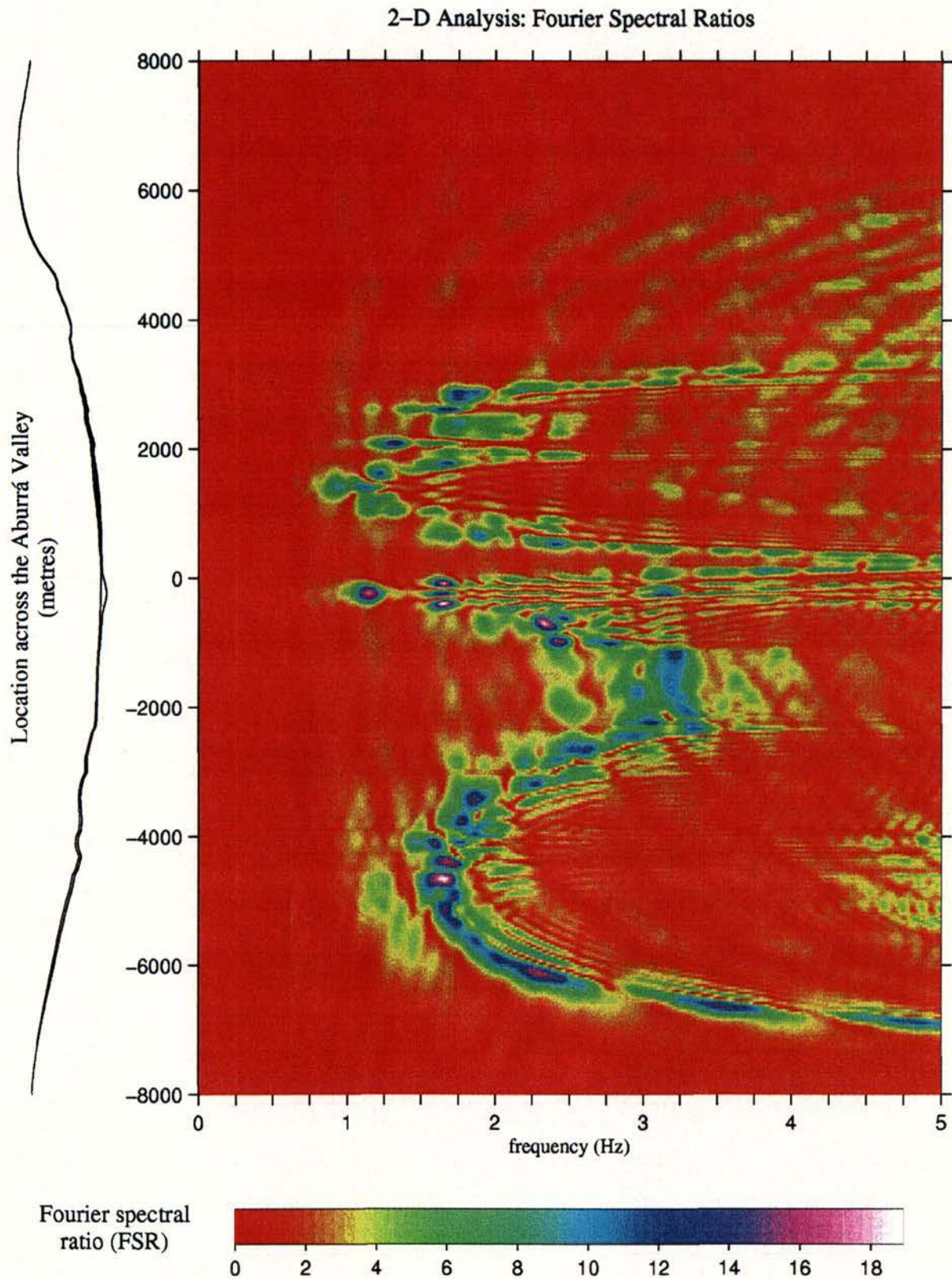


Figure 4.7. Fourier spectral ratios at the surface from the two-dimensional FEM analysis, plotted as a continuous function of position across the cross-section. FSR is shown as a colour scale.

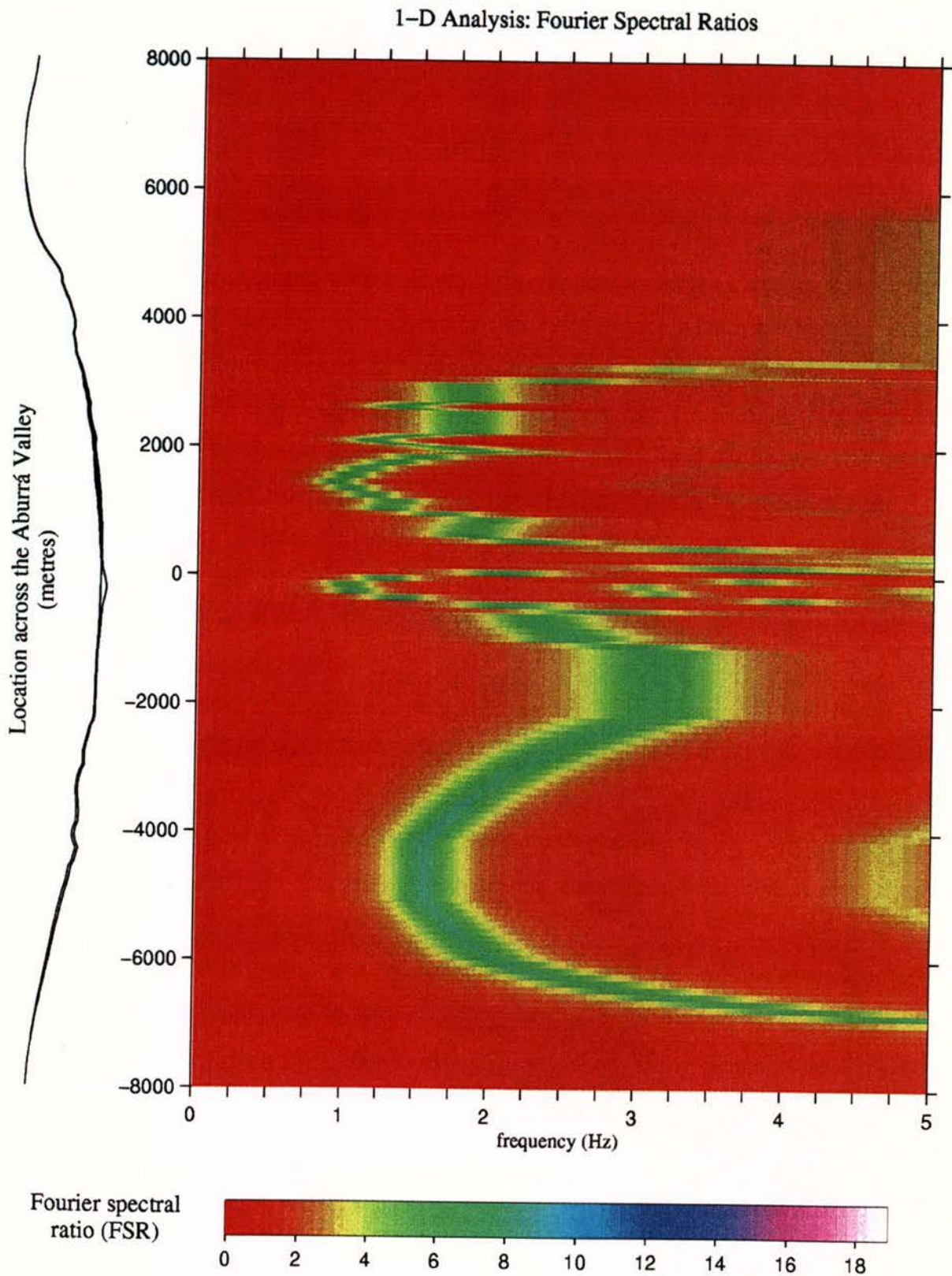


Figure 4.8. Fourier spectral ratios at the surface from the one-dimensional FEM analysis of two hundred points across the valley. FSR is shown as a colour scale that corresponds to the scale of figure 4.7.

of the one-dimensional analysis in figure 4.8, nor are they observed outside the zone of soft soil in the two-dimensional results. The origin of this pattern is possibly a weak whole-valley soft-soil response, or a whole-valley topographic response. It may also be influenced by the unwanted numerical reflections from the artificial boundary as described in section 4.1.4.

#### 4.2.2 *FREQUENCY RESPONSE IN THE REGION OF THE ACCELEROGRAPH STATIONS*

Figure 4.9 shows the Fourier spectral ratios for the 5km-wide region of the model between –1500m and +3500m, including the three accelerograph stations UEA, ISA and EET. Within the alluvial dip between –600m and +100m the spectral peaks show a clear pattern of two-dimensional resonance. A discussion on 2-D resonance patterns is presented in Adams et.al (1999). The very strong single peak at 1.15Hz and triple peak at 1.65Hz represent the 1<sup>st</sup> and 3<sup>rd</sup> horizontal resonant modes (respectively) of the 1<sup>st</sup> vertical resonant mode. The lower amplitude 5<sup>th</sup> and the 7<sup>th</sup> horizontal modes can also be seen at 2.10Hz and 2.40Hz respectively. At 3.15Hz a further centrally located ( $x = 250\text{m}$ ) peak indicates the onset of the 2<sup>nd</sup> vertical mode.

Two-dimensional resonance effects also occur in the thick layer of debris-flow and residual deposits between +300m and +3100m. Within this zone there appears to be a complex interaction of several resonance patterns of different size-scales. The largest of these is the full 2800-metre-width, which forms a (rather hypothetical) weak two-dimensional resonance pattern. Within this, the 1600-metre-width between +300m and +1900m forms a well-defined two-dimensional pattern. On an even smaller scale, the small deposits of Qfm at +2100m and +2600m generate small basin-resonances of their own. The horizontal resonance component within any of these patterns does not appear to be strong enough to generate a fully formed two-dimensional pattern; rather only the two-dimensional modes that coincide with the one-dimensional pattern are visibly amplified. At any point within the debris-flow deposits, it is difficult to determine how much of the response is due to resonance set up within the whole deposit or half of the deposit, or whether it is just a very local effect.

The site that models accelerograph station UEA (+200m) lies in a position whereby it escapes most of the resonant effects generated within both the large alluvial dip to the west, and the debris-flow deposits to the east. Some of these adjacent effects do however leak across to this site creating the highly irregular (yet low) FSR shown in figure 4.11. This site is so shallow

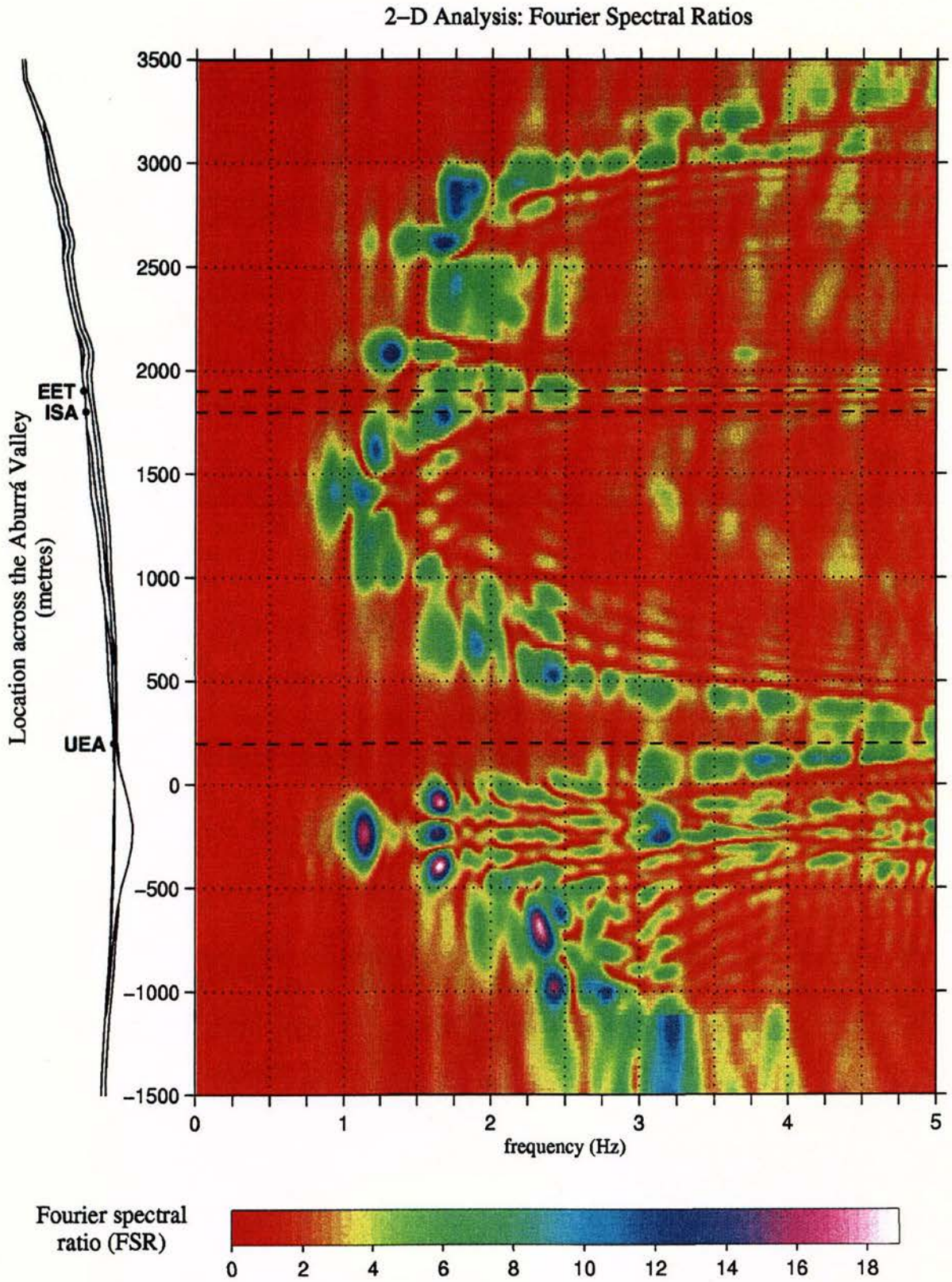


Figure 4.9. An expansion of figure 4.5 for the central-east 5km of valley, showing the locations of accelerograph stations UEA, ISA and EET.

that its fundamental vertical resonant frequency lies at around 6Hz, outside our domain of interest (0-5Hz).

Station ISA (+1800m) lies on the edge of the weak two-dimensional resonant pattern generated within the deposits between +300m and +1900m (described above). It has the misfortune to be located at the position of a strong, highly amplified anti-node in the pattern at a frequency of 1.7Hz.

The site of station EET (+1900m) appears to lie within the influence of two-dimensional effects from the basin-like structure of debris-flow deposits to the west, and also the thinner deposits immediately to the east. In addition to this, site EET is undoubtedly influenced by the small knoll of artificial fill shown in figure 3.11. On the lower plot in figure 4.11, there is three main peaks in the Fourier spectrum between 1.7 and 2.6Hz and a maximum FSR of 8.

### *4.3 COMPARISON WITH RECORDED DATA*

Fourier spectral ratios modelled at each of the three accelerograph stations on the cross-section (UEA, ISA and EET) are compared with Fourier spectral ratios calculated from weak motions recorded at these sites and also station ESE; which is sited on outcropping bedrock on the south-east quadrant of the Aburrá Valley.

#### *4.3.1 RECORDED WEAK MOTIONS*

Here we look at the response of each of the three stations of interest during nine different events that triggered the reference station ESE during the period between May 1997 and October 1998. These events are summarised in table 1. Five of these events originate from the deep Bucaramanga Nest, two from shallow events in the area south-west of Bucaramanga, while the final two originate from the southern Veijo Caldas Seismic Zone (see figure 2.1). In this report we will limit ourselves to the north-south (NS) component of motion recorded at the accelerograph sites as this corresponds with the out-of-plane motion modelled in the two-dimensional cross section.

Of the accelerograph stations shown in table 1, the lowest accelerations are generally found at station ESE on the rock. Accelerograph UEA located on only a shallow depth of alluvium,

however, also records comparable low peak values. In general terms, accelerograph EET records peak accelerations between 3 and 10 times larger than those at ESE, while accelerograph ISA records peak accelerations 2-3 times that of ESE.

Date	Time (UTC)	Lat (N)	Long (W)	Depth (km)	$M_L$	Seismic Source	Distance (km)	Peak NS Acceleration (cm/s <sup>2</sup> )			
								ESE	UEA	ISA	EET
11-May-97	18:17	6.74	73.18	150	5.8	Villanueva <sup>BM</sup>	309	1.1	0.8	3.0	8.6
11-Jun-97	07:07	6.81	72.96	160	6.0	Cepita <sup>BM</sup>	336	0.9	0.7	2.5	7.6
11-Jun-97	19:10	6.84	73.09	150	6.1	Los Santos <sup>BM</sup>	320	1.4	1.1	3.2	10.1
24-Jun-97	17:54	6.87	73.23	150	5.5	Zapatoca <sup>BM</sup>	307	0.9		1.4	
2-Sep-97	12:14	3.93	75.68	150	6.3	Roncesvalles <sup>VC</sup>	295	3.1	3.6	10.0	25.0
11-Dec-97	07:56	4.00	75.95	220	6.6	Génova <sup>VC</sup>	333	3.8		6.6	13.0
6-Mar-98	09:37	6.28	73.89	30	5.4	Cimitarra <sup>SH</sup>	186	8.8	2.5	9.5	30.0
8-Mar-98	04:59	6.30	73.88	30	5.4	Cimitarra <sup>SH</sup>	187	7.2	3.7	15.0	49.7
10-Oct-98	21:55	6.85	72.90	160	5.7	San Andrés <sup>BM</sup>	343	0.5	0.3		2.9

<sup>UM</sup> Bucaramanga Nest, <sup>VC</sup> Veijo Caldas Seismic Zone, <sup>SH</sup> Shallow event

Table 1. Seismological characteristics and peak recorded accelerations (north-south component only) at stations ESE, UEA, ISA and EET for nine distant earthquakes.

Using accelerograph station ESE as the reference rock site, Fourier spectral ratios have been calculated at the other three stations for the nine earthquakes in table 1. These are plotted in figure 4.7 along with a calculated average FSR for all nine earthquakes. The Fourier spectral ratios show some variation in amplitude between events, yet in general display similar peaks in frequency. Average peak FSR reaches only 2.4 for station UEA, 6.2 for station ISA, and a very large 27.3 for station EET. The peak FSR for an individual earthquake at station EET is 35.2 at an apparently highly resonant frequency of 3.0Hz.

#### 4.3.2 ACCELEROGRAPH STATION UEA

Figure 4.11 shows some correlation between the 2-D result and recorded events over the frequency range 0-3Hz. Although the many small peaks in this region do not agree, the range of FSR between 1 and 2 is comparable. The small peaks in this band are likely to be a result of resonance effects in adjacent deeper layers, rather than a fundamental frequency associated with the shallow depth of soil at this site. Above 3Hz, the recorded FSR at station UEA drops

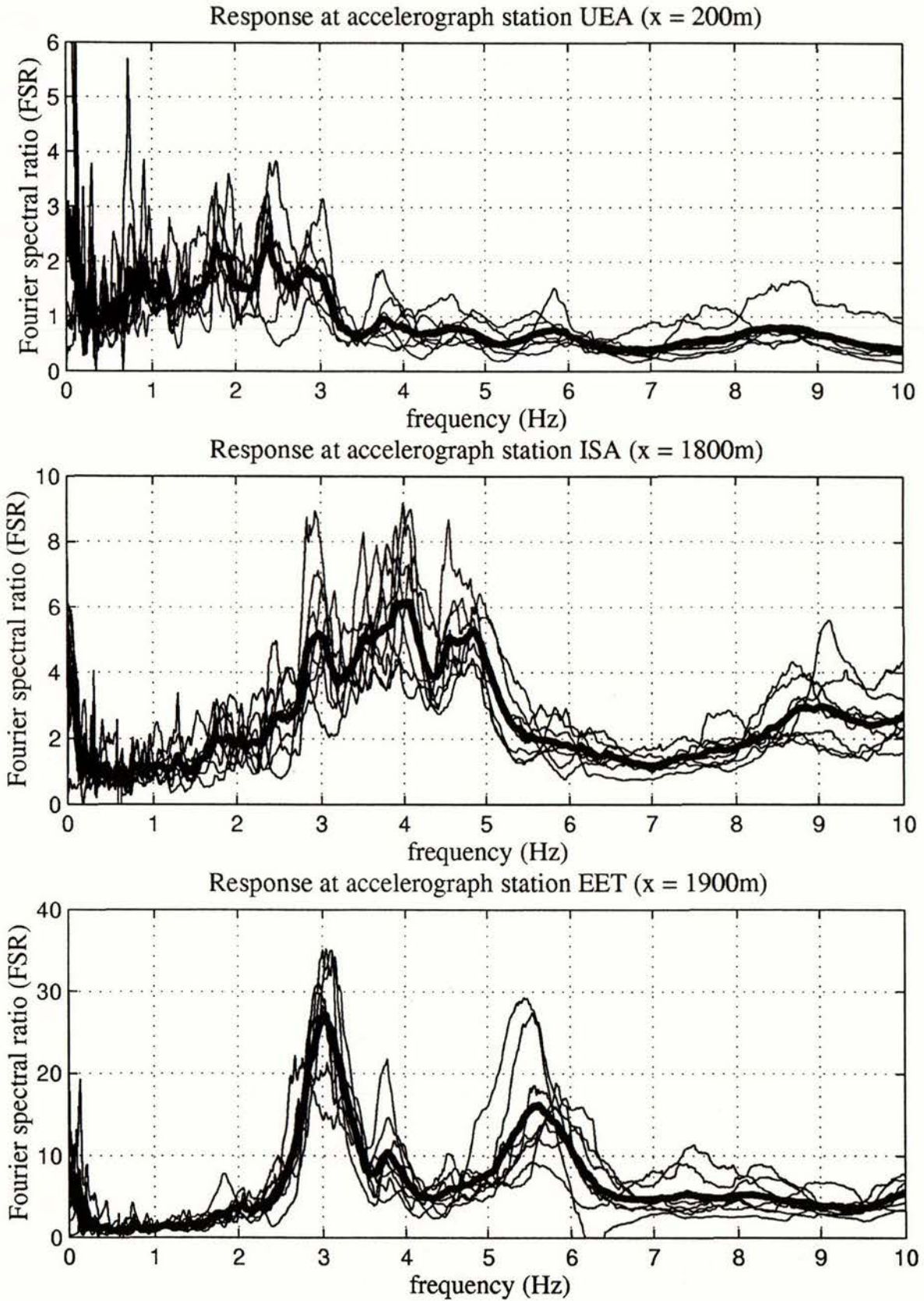


Figure 4.10. Fourier spectral ratios at stations UEA, ISA and EET for the nine different event shown in table 1. North-south components only. The average FSR is shown by the thicker line. Note that the FSR scale on the y-axis is different for each plot.

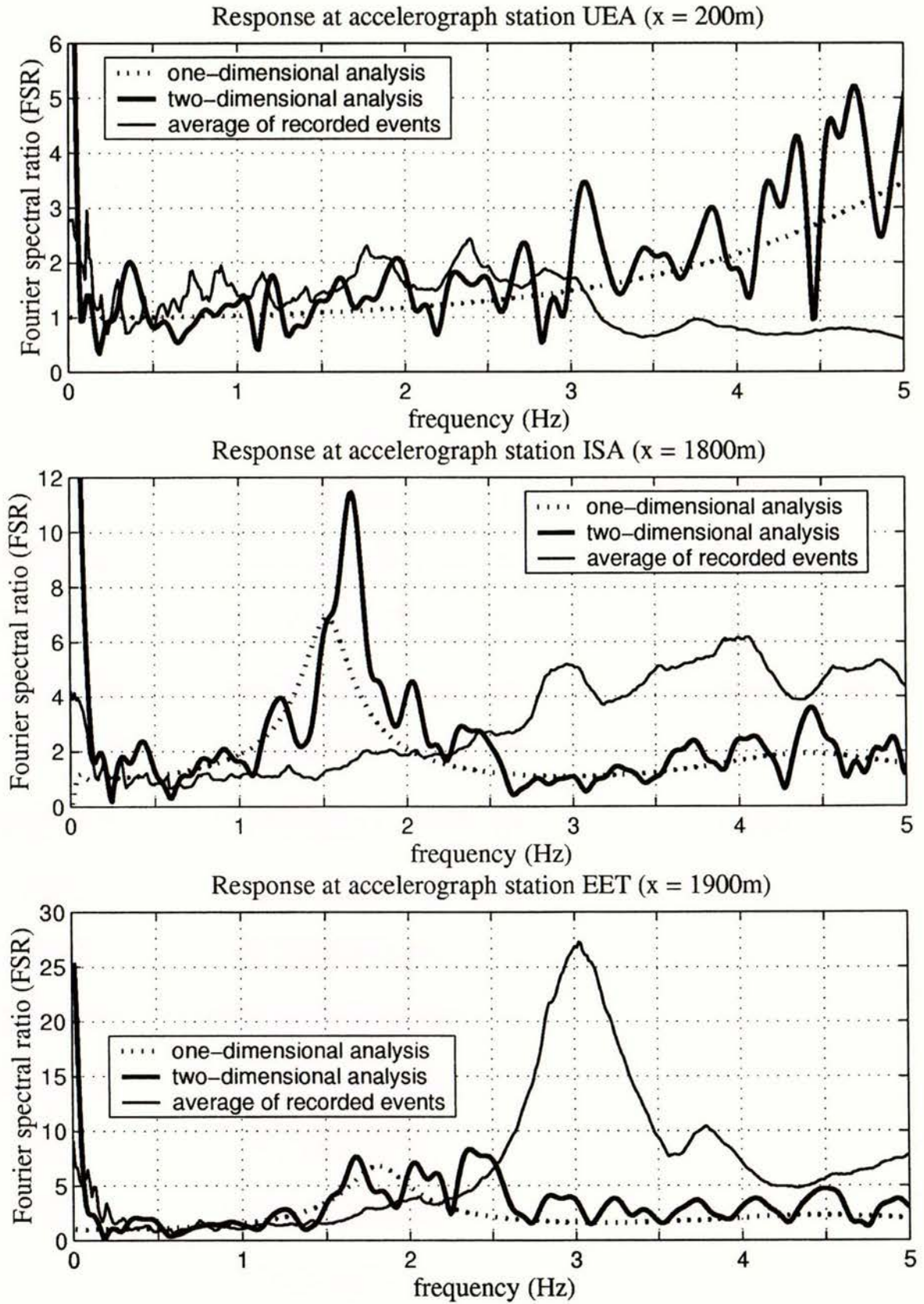


Figure 4.11. A comparison of Fourier spectral ratios obtained by one-dimensional (dotted line) and two-dimensional (dashed line) finite-element modelling, with an average FSR calculated from weak motions recorded at accelerograph stations UEA, ISA and EET. Note that the FSR scale is different for each plot.

below unity, indicating that the higher frequencies are amplified less at UEA than at ESE. Both our 2-D and 1-D models predict a fundamental frequency of around 6Hz at UEA, yet this is not shown in any of the recorded data.

#### 4.3.3 *ACCELEROGRAPH STATION ISA*

Both the 2-D and 1-D models predict a strong fundamental frequency of 1.5-1.7Hz at this site. Amplification from the 2-D analysis is significantly higher due to its misfortune of being located on an anti-node within a two-dimensional amplification pattern. Fourier spectral ratios calculated from recorded data at ISA, however, do not show this fundamental mode at all. Rather they show amplification of frequencies in the 2.5-5.0Hz band, up to a FSR of only five and six. On the whole, there appears to be little correlation between the modelling results and recorded data at this site.

#### 4.3.4 *ACCELEROGRAPH STATION EET*

At accelerograph station EET there appears to be a large discrepancy between recorded and modelled frequency spectra. Two-dimensional modelling predicts a wider and stronger band of amplification than the one-dimensional result for frequencies between 1.7 and 2.7Hz, yet neither is able to predict the very strong resonant frequency of 3.0Hz that is evident in the recorded motions. An average FSR of 27.3 for recorded motions at this frequency is obviously a result of something other than the one- and two-dimensional effects modelled in this study.

---

## Chapter 5: DISCUSSION

---

The Aburrá Valley at Medellín appears to have a very complex seismic site response; a product, essentially, of its highly irregular near-surface geology. The variable yet thin covering of soil within such a large valley means that the response of the valley as a whole is less important than response due to smaller-scale topographic and sub-surface features.

The geology of the Aburrá Valley is very unlike most of New Zealand. There are many different types of soft near-surface material, including residual soils, debris-flow deposits, alluvial deposits and artificial fills. The stratigraphy of these units is far from horizontal, with significant depths of soft material extending well up the sides of the valley. The boundaries between the geological units is sometimes very sharp (eg. between alluvial deposits and bedrock), but often more of a gradation (eg. between residual soil and bedrock).

The basement rocks are also of many different types, with several intrusive igneous bodies within older metamorphic units. While the spatial distribution and nature of surface geology has been carefully mapped; the depth, geometry and characteristics of the bedrock-soil interface are not understood in great detail. An indication of the possibly highly-irregular geometry of this interface is given by the Cerros Nutibara, Volador and Picacho and other hills of outcropping basement rocks, as well as a postulated tectonic structure through the centre of the valley. Thus, without a good understanding of the geometry of the basement, and a widely-spaced set of borehole logs providing information at only discrete points, we have employed a sometimes-dubious interpolation to create the two-dimensional model.

The abruptness of this interface between the competent basement rock and the overlying softer layers is undoubtedly a major contributor to the seismic response of the site. Residual soils invariably form a gradation from soft soil down to intact rock. And in fact the soil-rock interface is more of a transition than an interface. Davis (1995) shows how the weathered transition zone between residual soil and basement rock may have the effect of flattening the amplitude spectrum, especially at high frequencies. We do however, see evidence in roadway cuttings (eg. figure 2.4) that the transition from the soil material of low velocity ( $\sim 400\text{m/s}$ ) to that of a competent rock ( $\sim 2000\text{m/s}$ ) may in general be fairly abrupt, perhaps in the order of

one to two metres wide. The interface between various layers of debris-flow, alluvial and other deposits, is in most cases quite sharp as indicated from seismic velocity profiles, but not necessarily very regular or smooth.

Seismic velocity data from borehole tests indicate that the shear-wave velocity often increases gradually with depth within layers of similar composition. Davis and Hunt (1994) indicate that by taking an average shear-wave velocity and modelling each layer as homogeneous (as we have done in this study), it is likely that we somewhat under-estimate the amplification especially at higher frequencies.

In a complex geological situation of this type, the amplitude of the response at any point within the valley is dependent on the nature and geometry of the surrounding topography and sub-surface geology. This is called a multi-dimensional effect, as opposed to one-dimensional effects, whereby the amplification depends only on the depth and properties of soil below the site. Multi-dimensional effects may occur on both small and large geographic scales. For example, the amplification of a small deposit of artificial fill in an otherwise extensively flat terrain is most likely to be a function of the local nature of that fill, rather than the uniform surroundings; whereas the amplification at a site on a thick uniform deposit within a large steep-sided valley is more likely to be function of the geometry and nature of that valley, than of the locally uniform nature of the site.

In modelling the Aburrá valley with both one- and two-dimensional methods, we have shown that the seismic response at most locations is clearly due to a combination of one- two- and even three-dimensional effects. Multi-dimensional effects appear to exist on both small and large scales. Within the two-dimensional results, spatially variable and peaked amplifications of the first arrival of the Ricker wavelet is indicative of topographic and/or sub-surface stratigraphic focussing at many locations across the valley. Due to the relatively shallow depths of soil, this phenomenon is generally very local in nature. Other small-scale multi-dimensional effects observed in the Aburrá Valley model include strong horizontal resonance in small and well-defined soft deposits, and strong shaking of sharp topographic features such as the artificial deposit at station EET.

On a slightly larger scale, multi-dimensional resonance within sub-basin structures and thick soil deposits appears to influence the response across much of the valley. In the two-

dimensional modelling there is clear evidence of strong two-dimensional amplification both within the alluvial dip in the centre of the valley, and debris-flow deposits on the eastern slope. Neither of these structures is particularly well constrained in the horizontal direction, and for that reason the higher mode horizontal resonances are not well developed. The net effect is a spatially-peaked and highly amplified pattern of resonance occurring at frequencies similar to those from the one-dimensional analysis.

For any given site within the Aburrá Valley, it is therefore essential to consider a significant volume of surrounding geology in order to predict the seismic response at that site. Our results, however, show little influence from the overall large-scale dimensions of the valley. Rather, the structures within the valley on smaller scales from a few kilometres to a few metres wide appear to have the greatest influence on the results. These structures include well-defined dips and basins in the basement rock, localised thick depths of soft material that may act as resonators in the horizontal plane, and topographic features such as small side-valleys, gullies, banks, cliffs, sharp ridges and knolls. The incorporation of these features into a site-response model of the Aburrá Valley is crucial, while the incorporation of the whole valley is perhaps not quite so necessary.

The highly variable nature of the topography and near-surface geology exists in not only two, but all three spatial dimensions. Two-dimensional modelling has shown the nature and extent of the response due to the east-west horizontal dimensions of the valley and near-surface materials. As for the long-valley (north-south) dimension, the two-dimensional results have given an indication of its likely influence on the response. It appears that there will be little influence from the long-valley dimensions on a scale larger than 4-5km, yet on a smaller scale of order less than 1-2km, there may be significant effect from side valleys, ridges and horizontally discontinuous deposits. Thus, although two-dimensional modelling has produced substantial insights into the problem, it is not an adequate way to completely characterise site response within the Aburrá Valley. A three-dimensional study is undoubtedly essential for a more realistic solution.

The Aburrá Valley is very large both in height and width. The 18.6km-wide and 2.8km-deep finite element mesh contained 49,000 triangular elements and 102,409 nodes. A model of these dimensions is bordering on what is possible to analyse with Archimedes on a single 512MB processor (of course Archimedes may be run with much bigger problems on parallel

processors). The large topographic scale between the bottom of the valley (at 1500m amsl) and the surrounding hills (at 2600-2800m) also created several computational problems. The high degree of scattering within the wave field reflected down from the free surface has led to the errors generated at the absorbing boundary described in section 4.1.4. These errors are more pronounced due to the efficiently shaped lower boundary of the model that was selected as a compromise in the trade-off between accuracy and computational efficiency.

A comparison of the results of the modelling in this study with recorded data reveals very little evidence of any correlation between the two. This is an alarming result; however, it should be noted that the modelling in this study was carried out in a rather blind fashion. Fourier spectra at the three stations of interest were not studied in detail prior to the development of the cross-section model. Rather it has been based solely on the assumed geological-geotechnical model of the valley.

We can, however, hypothesise as to why the modelled results are significantly different to the recorded data. At accelerograph station UEA, the comparison is reasonable, except that the fundamental resonance mode at  $\sim 6$ Hz predicted in the modelling is not evident in the Fourier spectral ratios calculated from recorded data. In fact the FSR of site UEA is less than unity for frequencies above 3.2Hz. This result may be due to the high frequencies being filtered out during the FSR calculation by an abundance of high frequency motion at station ESE compared to UEA.

At accelerograph station ISA, the recorded data shows a group of peaks of lower FSR and at significantly higher frequencies than that in the modelling result. Although we might not expect to match the exact FSR of these peaks with the two-dimensional modelling, we would hope to be able to predict the frequency at which they occur. Because the site does not appear to have a locally complex three-dimensional nature, an accurate one-dimensional model should be able to predict the approximate resonant frequencies. A closer inspection of shear-wave velocity results at borehole P-21 (ISA) reveals that the homogeneous approximation of the 30m deep debris-flow layer (Qfs) is quite unrealistic and not overly representative of the measured data. While the top few metres are very soft, the material below 10 metres is much stiffer than is modelled. In addition, the residual soil below this may be much less weathered than is assumed due to its depth. The material properties adopted in the cross-sectional model, and shown in figure 3.9, are representative over the whole width of the Aburrá Valley rather

than at each particular site. An analysis with more site-specific data would undoubtedly give a better approximation of the recorded results.

At accelerograph station EET there is a large discrepancy between the recorded and modelled Fourier spectral ratios. In many ways, this extreme lack of correlation is not a complete surprise. The topography at station EET is highly irregular in both horizontal orientations, and the two-dimensional model used (figure 3.11) does not do justice to the site conditions. It seems most likely that the resonant frequency of 3.0Hz seen here is a fundamental mode of vibration of the small knoll of artificial and debris-flow deposits on which EET is sited. There may also be some influence from the large water-storage tank close-by, and larger-scale multi-dimensional effects due to the surrounding debris-flow deposit and bedrock geometries.

Although we can make few conclusions as to seismic site response for specific locations within the Aburrá Valley, this study has been highly successful in the sense that we have been able to identify the major contributors to seismic response. Two-dimensional modelling has shown the role, scale and influence of horizontal effects within the valley. The necessity to use highly accurate and site-specific data has been made evident for a valley with such an irregular and often thin covering of soil; such that there is perhaps a need for an even more detailed physical model of the near-surface geology. Meanwhile, the fact that the real response of the soil as registered by the accelerograph network is significantly different to the results obtained in this study, points to the indispensable value of the recording instruments.



---

## Chapter 6: CONCLUSIONS

---

The seismic response of the Aburrá Valley has been modelled with both one- and two-dimensional finite-element methods. The results have been compared both against each other in order to identify the dominant features of the valley that influence its response, and with weak motion data recorded at three different locations. The following conclusions have been made:

- There is some evidence of a two-dimensional whole-valley pattern of seismic response, yet its effect does not appear to be dominant or even particularly important to the response at any given site. Although highly variable in nature and depth, the soft soil covering within the valley appears to be too thin compared to the overall dimensions of the valley to produce a significant whole-valley response pattern.
- The response at a given site appears to be highly dependant on a intricate combination of one- two- and even three-dimensional effects, which occur as a result of large- and small-scale features of the immediate and surrounding topography and near-surface soft soils. The most influential features are usually less than a few kilometres across.
- At many sites across the valley, one-dimensional modelling correctly predicts the frequency of peaks within the Fourier spectrum, yet does not accurately define the value of FSR to be expected. The FSR values are often influenced by weak two-dimensional patterns of resonance set up within poorly-constrained soft units such as debris-flows.
- At sites that are very multi-dimensional on a local scale – such as at accelerograph station EET or within the alluvial dip in the centre of the valley – strong horizontal resonant modes may be present. Here, one-dimensional modelling is unlikely to predict the correct resonant peaks.
- Two-dimensional modelling gives a strong indication of whether or not the influence of horizontal effects will be significant in changing the amplitude (and perhaps frequency) of the peaks identified in a one-dimensional analysis.

- Two-dimensional modelling is generally not an adequate characterisation for much of the Aburrá Valley. The extent to which soil deposits and topographic features in the cross-valley orientation influence the response leads us to expect the same in the long-valley direction, where the geology and topography are also highly irregular. At some locations, however – such as the alluvial dip in the centre of the model where the long-valley geometry is more uniform – two-dimensional modelling is likely to be sufficient to define the resonant response.
  
- The results from the modelling in this study show poor correlation with recorded data at three different locations. This outcome points toward the need of a more detailed model of geometry and material properties to correctly predict even the elastic response at a given site. It also points toward the indispensable value of the Medellín accelerograph network.

---

## ACKNOWLEDGEMENTS

---

We are indebted to the assistance of Prof. Juan Diego Jaramillo and Luis Andrés Palacio (Ingeniería Civil, Universidad EAFIT, Medellín, Colombia) for both logistical and technical aspects of this study. Thanks to Gloria Maria Estrada (Geotechnical Engineer, Integrál SA, Medellín, Colombia) and Diego Rondón (Consulting Geologist, Medellín, Colombia) for several helpful discussions and ongoing technical support. Thanks to Leonardo Cano Saldaña, Hugo Monsalve and Mario De La Pava of the Universidad del Quindío in Armenia for their assistance and discussions regarding the 1999 Quindío Earthquake and Colombian tectonics. Muchísimas gracias to Amalia Cortavarria, Geraldine Jaramillo, Juan David Hincapié, Beatriz Elena Estrada, Amalia Urrea, Carolina and Ivonne Morales, Alvin Gongora, the Universidad EAFIT 1<sup>st</sup> XV Rugby team and all of the previously mentioned; who made Colombia a very friendly place.

Thanks also to Prof. Jacobo Beilak (Carnegie Mellon University, Pittsburgh, PA.) and Dr Jifeng Xu (Lam Research Inc.) for their support with the Archimedes computation.

This work was funded by the Earthquake Commission of New Zealand (EQC), the New Zealand Society for Earthquake Engineering (NZSEE), and the University of Canterbury.



---

## REFERENCES

---

Adams, B.; Davis, R.; Berrill, J.; Taber, J. (1999) Two-Dimensional Site Effects in Wellington and the Hutt Valley – Similarities to Kobe. *Civil Engineering Research Report*. University of Canterbury, Christchurch, N.Z.

Al-Hunaidi, M.O. (1989) Numerical Modelling of the Radiation Condition of Unbounded Media. In: *Engineering Seismology and Site Response: Proceedings of the 4th International Conference on Soil Dynamics and Earthquake Engineering*, Mexico City, Mexico, October 1989. Editors: A.S. Cakmak and I. Herrera.

Bao, H.; Bielak, J.; Ghattas, O.; Kallivokas, LF.; O'Hallaron, DR.; Shewchuk, JR. and Xu, J. (1998) Large-Scale Simulation of Elastic Wave Propagation in Heterogeneous Media on Parallel Computers. *Computer Methods in Applied Mechanics and Engineering*. **152**: 85-102. Elsevier Science S.A.

Bielak, J. and Christiano, P. (1984) On the Effective Seismic Input for Nonlinear Soil-Structure Interaction Systems. *Earthq. Eng. and Struct. Dyn.* **12**: 107-119.

Bielak, J.; Xu, J. and Ghattas, O. (1999) Earthquake Ground Motion and Structural Response in Alluvial Valleys. *J. Geotechnical and Geoenvironmental Engineering, ASCE*. **125** (5): 413-423.

Borcherdt, R.D. (1970) Effects of Local Geology on Ground Motion near San Francisco Bay. *Bull. Seism. Soc. Am.* **60** (1): 29-61.

Cartur (1998) *Medellin*. Relief map of Medellín City, 70cm x 100cm. Cartur, Santafé de Bogota.

Cremonini, M.G.; Christiano, P. and Beilak, J. (1988) Implementation of Effective Seismic Input for Soil-Structure Interaction Systems. *Earthquake Engr. Struct. Dyn.* **16**: 615-625.

Davis, R. (1995) Effects of Weathering on Site Response. *Earthq. Eng. and Struct. Dyn.* **24**: 301-309.

Davis, R. and Hunt, B. (1994) Amplification of Vertically Propagating SH Waves by Multiple Layers of Gibson Soils. *Intl. J. for Numerical and Analytical Methods in Geomechanics.* **18**: 205-212.

Escallón, J. and Alarcón, A. (2000) The January 25<sup>th</sup>, 1999 Earthquake in the Coffee Growing Region of Colombia – Tectonic and Seismological Aspects. *Proceedings of the 12<sup>th</sup> World Conference on Earthquake Engineering, Auckland, New Zealand.* Paper No. 2805.

Farbiarz, J.; Jaramillo, J.D. and Villarraga, M.R. (2000) Microzonation of the City of Medellín. *Proceedings of the 12<sup>th</sup> World Conference on Earthquake Engineering, Auckland, New Zealand.* Paper No. 2710.

García, L.E. (2000) The January 25, 1999, Earthquake in the Coffee Growing Region of Colombia: Accelerographic Records, Structural Response and Damage, and Code Compliance and Enforcement. *Proceedings of the 12<sup>th</sup> World Conference on Earthquake Engineering, Auckland, New Zealand.* Paper No. 2809.

García, L.E. (1984) Development of the Colombian Seismic Code. *Proceedings of the 8<sup>th</sup> World Conference on Earthquake Engineering, San Francisco, USA.*

Grupo de Sismología de Medellín (1999) *Instrumentación y Microzonificación Sísmica del Área Urbana de Medellín.* Informe para SIMPAD (Sistema Municipal de Prevención y Atención de Desastres) y Municipio de Medellín Secretaria Privada.

Grupo de Sismología de Medellín (1997) *Instrumentación y Microzonificación Sísmica del Área Urbana de la Ciudad de Medellín.* Informe Final (Versión detallado) con Adición CSA121 de Octubre 1998. Contrato C112 para SIMPAD.

Hincapié, J.E.; Osorio, R.; Pineda, C.M. and Urrea D.P. (1993) Hacia una Zonación Sismo-Geotécnica de Medellín. *Programa de Prevención Sísmica para Medellín, Segunda Etapa: Parte II.* PNUD, Alcaldía de Medellín. Universidad EAFIT.

- Hisada, Y.; Bao, H.; Bielak, J.; Ghattas, O. and O'Hallaron, D.R. (1998) Simulations of Long-Period Ground Motions during the 1995 Hyogoken-Nanbu (Kobe) Earthquake using 3D Finite Element Method. *Proc. 2nd Intl. Symposium on the Effect of Surface Geology on Seismic Ground Motion, Yokohama, Japan. Dec. 1-3, 1998.*
- Jaramillo, J.D. and Ortega, D.C. (1993) Estudio del Riesgo Sísmico de Medellín. *Programa de Prevención Sísmica para Medellín, Segunda Etapa: Parte III.* PNUD, Alcaldía de Medellín. Universidad EAFIT.
- Kellogg, J.N. and Dixon, T.H. (1990) Central and South American GPS Geodesy – CASA UNO. *Geophysical Research Letters.* 17 (3): 195-198.
- Monsalve, H. and Mora, H. (1999). Tectonica de Placas, Sismicidad y Deformacion en el Noroccidente Colombiano. In: *Terremoto del Quindío (Enero 25 de 1999)*. Informe Técnico-Científico, INGEOMINAS. Sec 1.3, 51p.
- Mora, H. (1995) Central and South America GPS Geodesy: Relative Plate Motions Determined From 1991 and 1994 Measurements in Colombia, Costa Rica, Ecuador, Panama and Venezuela. *M.S. Thesis, University of South Carolina, Columbia, 94 p.*
- Ricker, N. (1940) The Form and Nature of seismic Wavelets and the Structure of Seismograms. *Geophysics.* 5: 348-366.
- Shewchuck, J.R. (1996) Triangle: Engineering a 2D Quality Mesh Generator and Delaunay Triangulator. *First Workshop on Applied Computational Geometry (Philadelphia, PA.)*. pp 124-133, ACM, May 1996.
- Velásquez, E. and Jaramillo, J.D. (1993) Estudio de la Amenaza Sísmica de Medellín. *Programa de Prevención Sísmica para Medellín, Segunda Etapa: Parte I.* PNUD, Alcaldía de Medellín. Universidad EAFIT.

